Journal of Materials Chemistry A

ROYAL SOCIETY OF CHEMISTRY

REVIEW

View Article Online
View Journal

Cite this: DOI: 10.1039/d4ta00544a

Design and mechanism of photothermal soft actuators and their applications

Rajaram S. Sutar,[a] Sanjay S. Latthe,[ab] Xinna Wu,[a] Kazuya Nakata,[c] Ruimin Xing,[a] Shanhu Liu *[a] and Akira Fujishima[d]

Photothermal soft actuators have become a hot research topic in recent years due to the unique light-to-heat conversion, mechanical deformation, contactless operation, and extended applications from bionic design to intelligent robots. Moreover, since superhydrophobic surfaces offer drag reduction, anticorrosive, and oil absorption properties, the synergistic effects expand their smartness in micro-robots, environmental remediation, bioengineering, transportation, wireless delivery, and oil spill recovery applications. In this review, we have provided an overview of soft actuators based on the photothermal effect. We begin with a comprehensive overview of the photothermal conversion mechanism and the photothermal actuation mechanism. It explores three different types of photothermal actuation, discussing their design and mechanisms. Furthermore, we focus on the latest advancements in photothermal soft actuators, categorizing them based on actuation mechanisms and addressing their significance and associated challenges. The photothermal soft actuators enable bionic-like soft movement in the horizontal and vertical directions through bending, contraction, and rotation in response to light-induced heat. Then, this review introduces various applications of photothermal soft actuators. Finally, we draw insightful conclusions and expose exciting new possibilities in the field of photothermal actuators to create innovative solutions for photothermal soft actuators that will eventually benefit society.

Received 24th January 2024
Accepted 11th June 2024

DOI: 10.1039/d4ta00544a

rsc.li/materials-a

1. Introduction

The diverse plants and animals in nature exhibit unique characteristics and adaptability against complicated and inconsistent environments. Inspired by the unique features of plants and animals in nature, researchers have developed stimuli responsive actuating soft micro-robots like fish,[1,2] snakes,[3,4] mudskippers,[5] caterpillars,[6] and water striders.[7,8] Compared to conventional rigid actuators, soft actuators are flexible, lightweight, adaptable, bio-compatible, and have mechanically strong. A soft actuator is constructed from a stimulus-responsive material that transforms external energy into a specific form of energy, leading to the dynamic movement of the actuator. In the past decade, extensive research has been conducted on actuators that respond to external stimuli, namely pH,[9] humidity,[10,11] temperature,[12,13] light,[14,15] and electrical[16,17] and magnetic field.[18,19] Chemical stimuli actuators exhibit broad responsiveness but lack specificity, resulting in unintended actuation. They may have slow response and irreversible behavior, limited reversibility, and susceptibility to environments. Material selection is constrained by chemical compatibility, and they often require significant energy input, leading to high operational expenses.[20–22]

Temperature-responsive actuators are sensitive to ambient temperature changes, but their performances were often influenced by external factors such as fluctuations in environmental temperature. They operate within limited temperature ranges and require energy input for actuation. Their uniform actuation may limit precision in localized applications and make them sensitive to environmental conditions.[6,23,24] Electrically stimulated actuators often necessitate high voltages to achieve significant deformations or forces, which could increase complexity and expenses. Rapid actuation and precise control may lead to increased energy consumption and complexity.[25,26] Magnetic stimulus actuators are constrained by limited actuation ranges and reliance on an external magnetic field for operation, which might impede their portability and usability. Their actuation speeds are relatively slower and often vulnerable to interference from external magnetic fields. Their rigid construction restricts their flexibility and adaptability.[27,28]

In contrast, light-responsive actuators allow for non-invasive and wireless control, as they can be activated from a distance without physical contact. These actuators offer precise spatial

[a]College of Chemistry and Molecular Sciences, Henan University, Kaifeng 475004, PR China. E-mail: liushanhu@vip.henu.edu.cn

[b]Department of Physics, Vivekanand College (Empowered Autonomous), Kolhapur, 416003 Maharashtra, India

[c]Division of Sciences for Biological System, Institute of Agriculture, Tokyo University of Agriculture and Technology, 2-24-16 Naka-cho, Koganei, Tokyo 184-0012, Japan

[d]Tokyo University of Science, 2641 Yamazaki, Noda, Chiba, 278-8510, Japan

and temporal control by manipulating the intensity, wavelength, and duration of light exposure. They are constructed using materials such as polymers, hydrogels, and nanocomposites, providing flexibility in both design and performance. With rapid response and low energy input, they can be activated from a distance using light sources like lasers, LEDs, or natural sunlight and find applications in robotics, optical devices, and microfluidic systems. Based on light manipulation, researchers have proposed three types of actuations using photoresponsive materials based on photochemical,[29,30] photoelectrical,[31,32] and photothermal[33,34] effects.

As for photochemical effects, actuation occurs through changes in molecular structure, such as photodimerization and photoisomerization. Photochemical molecules can undergo transformations such as isomerization, cycloaddition, dimerization, and ionization reactions.[35–39] Generally, photochemical actuators have been developed using azobenzene, spiropyran, diarylethenes and polyacrylamide gels.[40–42] For example, azobenzene derivatives, when exposed to UV radiation, would undergo *cis–trans* isomerization, which leads to significant molecular distortion. Spiropyran and diarylethenes undergo a ring-opening reaction upon UV-light exposure; and the ring-closure process can be achieved through thermal relaxation or irradiation with visible-light. These changes happen at a nanoscopic level or within seconds, which cause lower bending degrees,[43] or even poor dynamic performance in actuating micro-robots.[44]

As for photoelectrical effects, the semiconductors (especially silicon) generate photoinduced electron–hole pairs with crystal lattice distortion, leading to cantilever bending.[45] Likewise, graphene moves forward or propels itself by virtue of emitting electrons when exposed to simulated sunlight. But when the light source is changed to laser beams, the generated electrons might impart a recoil force that leads to the displacement of graphene, since this force is significantly greater than the force produced by radiation pressure.[46] Graphene sheets exhibit a unique cone-shaped band structure without any gaps. The dynamics of photoexcited charge carriers in graphene sheets are influenced by Auger-type processes. Oxygen functional groups in 3D bulk graphene create electronic barriers and a localized bandgap. When the photon energy is greater than the bandgap, it can release free hot electrons to propel itself.[47,48] However, the prepared photoelectric actuators still face some challenges, such as fabrication difficulties and specific light sources.

The photothermal effect is an alternative technique to induce actuation *via* photoinduced heat. Herein, photothermal materials with excellent light absorption capability and thermal conductivity are usually selected to ensure the performance of photothermal actuators. Therefore, photothermal actuation has the following unique advantages. Firstly, it avoids potential photochemical side effects that result in fatigue. Secondly, it can absorb a wide range of light spanning the whole solar spectrum. Lastly, heat can diffuse into the entire material beyond the limited photon penetration depth.[49] Moreover, photothermal actuators have simple design principles, controllable reconfigurations, wide adaptability, fast response, and outstanding stability. Fig. 1a depicts published articles on the topics of photochemical, photoelectrical, and photothermal effects over the past 24 years. Meanwhile, Fig. 1b displays the escalating trend in publications and citations of photothermal actuators from 2001 to the present, underscoring the widespread interest in the development of such actuators. The remarkable advancements in photothermal actuators can be attributed to the uniform dissemination of photo-induced heat into the entire material, straightforward design principles, and precise control of actuation by the specific intensity or wavelength of light from a distance.

Inorganic and organic photothermal materials are the two main categories. Inorganic photothermal materials such as metallic nanoparticles and semiconductors, are known to have high photothermal conversion efficiency and excellent physical and chemical stability. Organic photothermal materials include carbon-based and polymeric nanomaterials, in which polypyrrole (PPy) and polydopamine (PDA) are often used in polymeric matrices.[50] When a photothermal material is exposed to light on a liquid surface, it induces heat that is transferred to the surrounding liquid, creating a gradient in surface tension. This surface tension gradient results in the movement of an

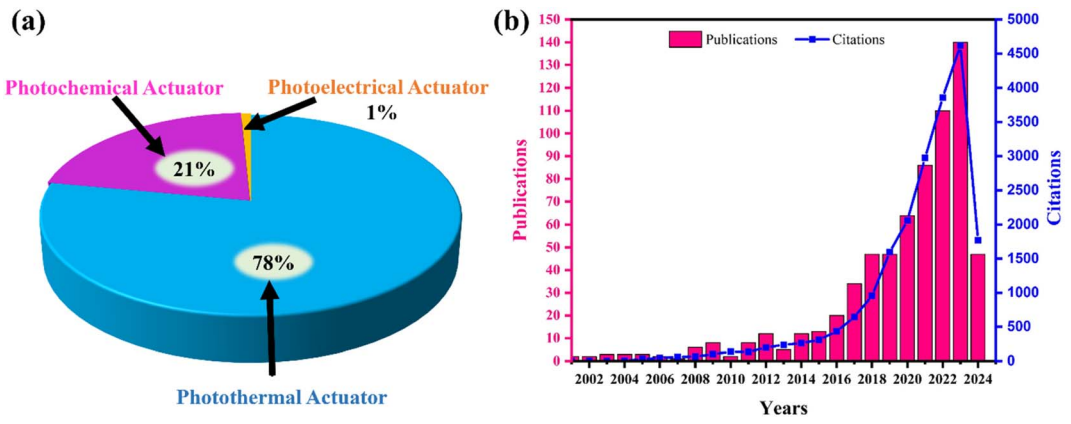

Fig. 1 (a) Articles published on the topics of photochemical actuators, photoelectrical actuators and photothermal actuators. (b) Number of publications and citations of photothermal actuators (source: Web of Science, 28 May 2024).

actuator on the liquid surface.[51] The photothermal actuators are composed of materials having different coefficients of thermal expansion (CTE), which cause the light responsive expansion or contraction of the material.[52,53] Generally, these types of actuators are designed by combining layers of lower and higher CTE materials. The photoresponsive components such as MXenes,[54,55] graphene,[56,57] carbon-based materials,[58] and graphene and their derivatives[59,60] have lower CTE and are used as a light absorption layer. Polymers such as polydimethylsiloxane (PDMS),[61,62] polyvinylidene fluoride (PVDF),[63] polyethylene (PE),[64] and polycarbonate (PC)[65] have high CTE and are used as thermal expansion layers. The high CTE layer expands asymmetrically due to heat generated by the low CTE layer upon exposure to light.[66–69] Some polymers, for example shape memory polymers (SMPs)[70–72] and liquid-crystal elastomer (LCEs),[73–75] exhibit temperature-dependent phase transition such as anisotropic/isotropic transition and glass transition. When these polymers combined with the layer of photothermal materials, temperature can be increased under light irradiation. The mesogen alignment in the LCEs (nematic phase) becomes disordered when temperature increases beyond the isotropic phase transition temperature (T_{trans}), resulting in a shape change. Once the light source is removed and the material cools down, LCE regain their original shapes.[76,77] Similarly, SMPs exhibit shape change in response to temperature. They can be set into a temporary shape at temperatures below T_{trans}, and then return to their original shape when heated above T_{trans}.[78,79] Generally, photothermal actuators are operated by visible light (vis),[80–84] near-infrared (NIR),[56,85–89] ultraviolet (UV),[90–93] and sunlight.[94–96] To achieve multifunctionality, photothermal actuators can be designed by integrating self-healing and superhydrophobic properties.[33,34,97] Photothermal actuators have shown fast response and outstanding performance in oil-spill recovery,[98] microplastic collection from water,[99] switches,[100] cargo delivery,[101] nanogenerators,[102] and sensors.[103] Recently a US patent was registered in 2021 for photothermal actuators; they have dip coated nylon fibers with graphene flakes that revealed bending under laser light irradiation.[104]

Several comprehensive reviews of photo-actuators have been published, providing an overview of different types of photo-actuators and their development.[105–109] In recent years, there has been considerable research into the development of

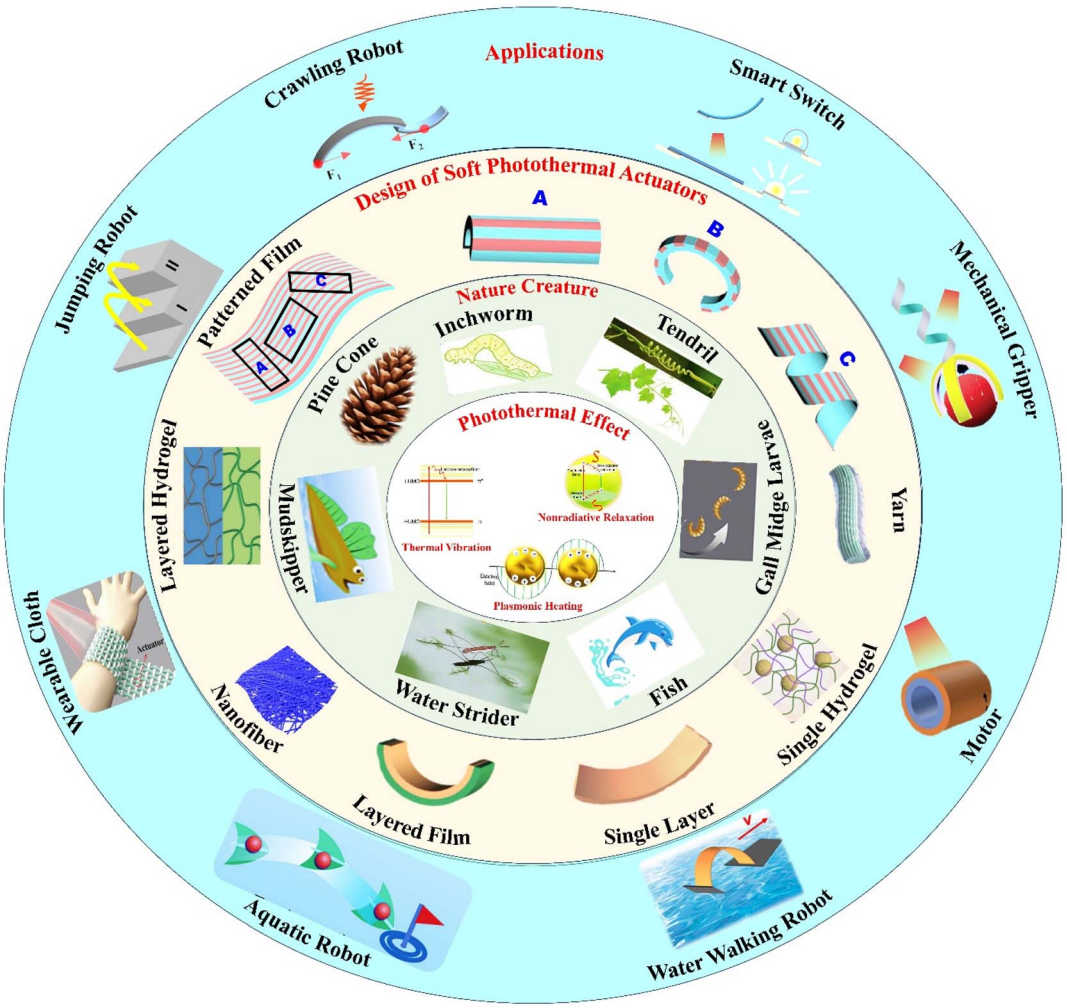

Fig. 2 Overview of photothermal conversion mechanisms, natural creatures, design of photothermal actuators, and their potential applications.

photothermal actuators. This review provides a comprehensive overview of the photothermal conversion mechanism, the selection criteria for photothermal materials for the design of photothermal actuators, and their relevant applications. In Fig. 2, a comprehensive illustration of the basic principles of photothermal conversions, natural inspirations, and design strategies for photothermal actuators is provided. This encompasses various actuation mechanisms and their diverse associated applications. This review begins with an overview of various photothermal materials with a focus on their characteristics and absorption capabilities. Subsequently, this article discusses the three different types of photothermal actuation, focusing on their design and mechanisms. Thereupon, we shift our attention to the latest advancements in the field of photothermal actuators, categorized according to their actuation mechanisms. It further discusses the potential of integrating superhydrophobic properties with photothermal actuators to enable intelligent actuation in aquatic environments. In the conclusion section, we present our insights on the existing challenges and future developments in the realm of photothermal actuators.

2. Fundamentals of photothermal actuation

Photothermal actuators typically rely on the photothermal effect, where a photothermal material absorbs light energy, resulting in localized heating. This heating produces temperature and surface tension gradients on liquid surfaces, and expansion/contraction and phase transitions in thermo-responsive materials, leading to actuator movement. To understand the process of light energy conversion into dynamic movement of an actuator, it is essential to comprehend the theoretical background and conversion mechanism. This section briefly discusses the photothermal conversion mechanism and the photothermal actuation mechanism.

2.1. Photothermal conversion mechanism

Photothermal conversion is a process that converts light into heat, and it can be observed in various materials, including noble metals, semiconductors, and organic materials.[110] The choice of light source depends on the specific requirements of the experiment or device. Various light sources, including vis, IR, NIR, UV, and focused sunlight, are commonly used for photothermal actuation. The photothermal effect is significantly influenced by factors such as wavelength and intensity of light. Lasers are often preferred due to their coherence, monochromaticity, and high-intensity light. Different materials have specific absorption spectra, so the choice of wavelength can be tailored to optimize the photothermal effect. Higher light intensities can lead to more significant heating effects. The process of electromagnetic radiation interacting with matter and converting light into heat can be categorized into three primary mechanisms: plasmonic localized heating (PLH) of metals, non-radiative relaxation (NRR) of semiconductors, and thermal vibration of molecules (TVM).[50,111]

In plasmonic localized heating, metallic nanostructures contain a high density of free and polarizable electrons, which can absorb photon energy through electron transitions. After being photoexcited, the localized surface plasmon resonance quickly enters a nonequilibrium state, leading to rapid dephasing and decay. The energy absorbed by electrons can be dissipated *via* the emission of photons or electron–hole pair generation through Landau damping, ultimately returning to a thermally equilibrated state.[112,113] The rapidly dissipating nonradiative plasmon produces high-energy electrons. The low-energy electrons rapidly interact with one another and generate thermal energy. Finally, the metallic structure ultimately dissipates its thermal energy to the surrounding environment *via* phonon–phonon collisions.

Non-radiative relaxation in semiconductors can also display photothermal effects through direct interband/intraband electron transitions. When a semiconductor absorbs photons, it generates electron–hole pairs. The energy from these pairs can undergo non-radiative relaxation, leading to a localized increase in temperature as it is transferred to the material's lattice.[114] The heat generation in semiconductors arises from the Shockley–Read–Hall and Auger recombination processes.[115] Organic materials exhibit excellent light absorption and can produce heat through lattice vibrations. When organic materials are exposed to low energy, loose electrons can be stimulated from the π orbitals to the π^* orbitals. The material undergoes an electronic transition when the energy of incident photons is sufficient, and excess energy is emitted as heat. The disparity in energy levels between the highest-occupied molecular orbital (HOMO) and the lowest-unoccupied molecular orbital (LUMO) reduces with an increase in the number of π bonds.[111] Table 1 summarizes the challenges and limitations of different photothermal materials.

In designing photothermal actuators, light absorption and conversion efficiency of photothermal materials are essential factors. The careful choice of materials and innovative design of nanostructures play a crucial role in maximizing light absorption. The primary process of photothermal conversion is light absorption, which can be improved by minimizing the transmittance and reflectance of the material. The nanostructure can be designed with single or multiple photothermal components, and different photothermal conversion mechanisms. Nanomaterials exhibit distinct thermal, optical, and electronic characteristics, rendering them highly suitable for photothermal conversion applications.[130] Furthermore, 2D and 3D structured photothermal materials have strong light absorption capability and consequently generate higher heat conversion efficiency.[131–133] Plasmonic metal nanostructures have large absorption cross-sections and can convert light into heat through localized surface plasmon resonances.[134] Nanostructured semiconductors like metal oxides and chalcogenides can improve the photothermal conversion efficiency by bandgap engineering or free-carrier-induced localized surface plasmon resonances.[135,136] Nanomaterials based on carbon and polymers can absorb a wide range of light across the solar spectrum and transform it into heat by exciting electrons from the π orbitals to the π^* orbitals through conjugation and hyperconjugation effects.[137,138] However, certain materials exhibit photophysical activities, photochemical

Table 1 Challenges and limitations of photothermal materials based on their conversion mechanism

Photothermal conversion mechanism	Materials	References	Design	Performance	Challenges	Limitations
Plasmonic heating	Au, Ag, Cu, Pt, Pd, *etc.*	116–120	Tuning the size and structure of the materials; coating with stabilizing agents, doping with other metals	Expands the absorption range and photothermal conversion efficiency	• The aggregation in the polymer matrix reduces conversion efficiency • Complexity in the synthesis of nanomaterials • Heat affected limited region • Prone to oxidation and corrosion	• Penetration depth of the incident light • Specific wavelength of light absorption • Toxicity • Expensive • Poor thermal stability • Heat dissipation • Short lifespan under continuous illumination
Non-radiative relaxation	Semiconductor and transition metal oxides (MnO_2, Fe_3O_4, CuS, WO_3), quantum dots (CdSe, PbS) *etc.*	121–126	Adding impurities or introducing disorder to the nanomaterials; creating heterojunctions; surface modification	Extends the absorption range and photothermal conversion efficiency; improves charge carrier dynamics	• Complexity in synthesis • Controlling the band gap of semiconducting materials • The aggregation of materials during synthesis reduces conversion efficiency • Sensitivity to environmental conditions	• Adverse effects on the environment • Toxicity • Expensive • Pure materials only responsive to UV light • Photobleaching • Limited long-term stability
Thermal molecular vibration	Carbon materials and their derivatives (graphene, CNTs, fullerenes), organic dyes (NIR dyes), conjugated polymers (P3HT, PEDOT:PSS), *etc.*	52 and 127–129	Adjusting porosity with 1D, 2D and 3D structure of the materials; chemical functionalization, composite formation	Increases the absorption range and photothermal conversion efficiency, enhances mechanical properties	• Complexity in preparation • Difficulties in adjusting optical transparency • The aggregation or addition in the polymeric materials reduces conversion efficiency • Enhances mechanical properties	• Long-term exposure to light causes organic dye and polymer to photodegrade • Requires high intensity light • Some carbon materials are expensive • Poor stability • Limited recyclability • Potential health hazards

reactions, reversible mechanical deformation, and photovoltaic reactions when exposed to light.[139–141] Photophysical activities impact light absorption and scattering, while photochemical reactions alter the bonding structure of materials, thus affecting the photothermal response. Photomechanical and photovoltaic effects play a role in material deformation and localized heating, respectively.

2.2. Photothermal actuation mechanism

2.2.1. Surface tension gradient. When a beam of laser light is directed toward the photothermal actuator located at the interface between water and air, it causes heat at the targeted location, subsequently producing a temperature gradient. When the temperature of water rises, it creates a gradient in surface tension. Hence, low surface tension molecules become attracted to the water molecules with high surface tension, resulting in the propulsion of an actuator.[142,143] The photothermal materials generate heat by absorbing light, raise the water temperature and create a gradient in surface tension. This gradient enables actuator to be propelled from the lower to higher surface tension region.

The light-induced pressure (F) considered for actuation is expressed by the following equation,[144]

$$F = \frac{p}{t} = \frac{E}{Ct} = \frac{P}{C} \quad (1)$$

where p, t, E, C, and P are the momentum, time, energy of light, speed, and power of light, respectively. Compared to the gravitational force acting on the actuator, light-induced pressure is lower and it is insufficient to drive the actuator. However, in the irradiated region of the actuator the temperature is higher than that of the surroundings; it produces a temperature difference, resulting in a surface tension gradient. The surface tension difference enables the movement of low surface tension liquid molecules toward the region of higher surface tension. The temperature-dependent surface tension discrepancy is given by the Harkins formula as follows,[95,145]

$$e = b_0 + b_1T + b_2T^2 \quad (2)$$

where e represents the surface tension (mN m^{-1}), $b_0 = 75.796$ mN m^{-1}, $b_1 = -0.145$ mN m^{-1} °C^{-1}, $b_2 = -0.00024$ mN m^{-1} ° C^{-2} (these are constants), and T is the temperature (°C).

2.2.2. Expansion/contraction. When layered photothermal actuators made of materials with different CTE are exposed to light, they expand and contract. These expansions and contractions produce subsequent bending movements, which cause bionic actuation. In a layered structure, a passive layer of low CTE that can absorb light and high CTE serves as the thermal expansion layer. The bending movement of layered photothermal actuators can be explained by beam theory,[146,147]

$$\frac{1}{R} = \frac{6E_1E_2a_1a_2(a_2 + a_1)(\alpha_2 - \alpha_1)\Delta T}{(E_1a_1^2)^2 + (E_2a_2^2)^2 + 2E_1E_2a_1a_2\,(2a_1^2 + 3a_1a_2 + 2a_2^2)} \quad (3)$$

where R is the curvature radius of the deformation of the layered film; the elastic moduli of layer 1 and layer 2, their thicknesses, and CTEs are denoted by E_1 and E_2, a_1 and a_2, and α_1 and α_2. ΔT is the temperature change. Simplifying this equation by determining some variables,

$$\frac{a_1}{a_2} = x,\ \frac{E_1}{E_2} = n,\ \text{and } a_1 + a_2 = h \quad (4)$$

Therefore,

$$\frac{1}{R} = \frac{6(\alpha_2 - \alpha_1)\Delta T(1 + x)^2}{h\left[3(1 + x)^2 + (1 + xn)\left(x^2 + \frac{1}{nx}\right)\right]} \quad (5)$$

Eqn (5) indicates the larger ΔT and difference between the CTEs of layers can achieve greater actuator deflection. Hence,

$$\frac{1}{R}\alpha(\alpha_2 - \alpha_1)\Delta T \quad (6)$$

2.2.3. Phase transition. Some reactive polymers, for example LCEs and SMPs, undergo phase transitions (anisotropic/isotropic transition or vitrification/glass transition) when exposed to light by converting light energy into mechanical work. These phase transition processes cause actuation by storing and releasing large amounts of energy. In LCEs, mesogens align in a polymer network at room temperature (they are in a nematic phase), but they become disordered when the temperature exceeds the isotropic phase under light irradiation (they are in an isotropic liquid phase), subsequently its volume decreases. As a result, the film contracts along the direction of the mesogens at the above T_{trans} and expands after cooling.[148–150] Recently, the photothermal components like carbon nanotubes (CNTs) and graphene oxide (GO) were incorporated into the LCEs to enhance actuation performance.[151,152] SMPs can be deformed by applying force above T_{trans} and regain pre-programmed shape upon cooling below T_{trans}.[11,153,154] The addition of photothermal components can enhance the actuation performance of SMPs.

3. Recent strategies for designing photothermal actuators

Since the performance of a photoactuator depends on the strategic coupling between photothermal and thermal–mechanical conversion, the photothermal conversion components play a crucial role in driving photoactuators through the photothermal effect. Recently, materials such as CNTs, GO, Au, MXenes, and PDA have been effectively utilized as photothermal materials due to their high photothermal conversion ability and thermal conductivity. In this section, we discuss the three categories of photothermal actuation mechanisms: surface tension gradient, expansion/contraction, and phase transition-based actuation, and briefly mention the progress in developing photothermal actuators.

3.1. Surface tension gradient

A surface tension gradient on the liquid can be produced by a light-induced photothermal material that generates heat and

transfers it to a localized liquid. As a result, photothermal objects move forward from the region of low surface tension and cause dynamic movement on the liquid surface. Generally, focused sunlight or laser light generates a thermal surface tension gradient on the liquid surface. Okawa *et al.* have fabricated a light-responsive actuator by combining vertically aligned carbon nanotubes (VACNTs) as photothermal material with a PDMS block.[155] Under light illumination, the VACNTs generate heat and hence the surface tension of liquid fluctuates, leading to the linear or rotational motion of the actuator. The light-driven actuator can be driven over the surface of various liquids such as water, alcohol, glycerol, and dimethyl formamide. Maggi *et al.* have developed photothermal asymmetric microgears, irradiated by blue LED light, and achieved rotational motion on the liquid surface.[156] Xiang *et al.* have prepared a PDMS/GO layered light-driven mudskipper-like bionic robot.[5] Under laser light irradiation, the bionic actuator creeps on the liquid and bends in air. The PDMS exhibited higher CTE (3×10^{-4} K^{-1}) than GO which has a negative CTE (-10^{-4} K^{-1}). The GO absorbs light energy and generates localized heat. The increased temperature generates internal stress between PDMS and GO, leading to bending toward the GO side. Under periodic light irradiation, it produces reversible bending/unbending motion. The presence of a photothermal GO layer changes the surface tension of water after laser light illumination that causes it to propel the actuator in the forward direction. The PDMS/GO actuator jumps up from the ethanol solution like a mudskipper jump from the air/ethanol interface. However, effectively controlling the direction and enhancing the actuation speed of the conventional photothermal aquatic robot is challenging due to the homogeneous light-induced heat diffusion at the liquid surface.

To address this issue, Liao *et al.* have utilized aligned one-dimensional photothermal nanomaterials to create light-driven motors.[157] A light-propelled motor was created by sticking a one-dimensional aligned multi-walled carbon nanotube (MWCNT) film to the PDMS block (see Fig. 3a). This design facilitates rapid localized propulsion with high spatial resolution. Under NIR laser light (20 W cm^{-2}) illumination, MWCNTs produce heat, which is transmitted to the liquid surface, creating a surface tension gradient that propels the motor forward. The heated surface returns to its original state once the motor has passed, without introducing any intermediates to the system. The direction of its propulsion was controlled by the position of light irradiation on a vertically aligned MWCNT film. In order to assess the transport capabilities of an actuator, two pieces of MWCNT film were affixed vertically to both sides of a PDMS block with a cargo loading space. The iron foil loaded on a ship as cargo drove by light to the targeted spot in a curved motion as seen in Fig. 3b. The ship came back along a curvilinear route after dropping the iron foil using a magnetic holder. The motor can move linearly at a speed of 4.19 cm s^{-1} and rotationally at 5.3 rad s^{-1} (Fig. 3c).

However, the above-discussed actuators can float on a 2D liquid–air or liquid–liquid interface, which limits the further application of actuators. Zhou *et al.* have prepared a driven micromotor using a reduced GO aerogel.[160] Under laser light irradiation, the motor traveled vertically beneath the water and horizontally on the surface of the water. Pan *et al.* have introduced photothermal nanoparticles (CuS nanoparticles) into temperature-responsive hydrogel poly(*N*-isopropylacrylamide) (PNIPAM) to develop a transparent light-driven moveable actuator (LTMA) that can move over a liquid in three dimensions when exposed to NIR laser light or sunlight.[158] Fig. 3d illustrates the actuator floating toward the liquid–air interface when the actuator is irradiated by laser light.

The light irradiation position could be changed to alter the LTMA's motion direction. Like controlled motion of LTMA on the liquid–air interface, their motion can be controlled in 3D motion under liquid by light irradiation. Interestingly, their hydrophobicity can be controlled by light. When light is turned off, LTMA absorbs the surrounding liquid and sinks to the bottom. Fig. 3e shows that the controllable 3D motion of LTMA by avoiding the obstacles. In this, obstacles were fixed at the liquid–air interface and LTMA moved under obstacle by utilizing the floating and sinking ability of LTMA. Further, LTMA was used in the sampling process. As shown in Fig. 3f, the LTMA can drive to the target area to absorb the target molecules and then drive back. Hence, it confirms that LTMA can move on the liquid–air surface as well as in the liquid under light illumination. In another study, Chen *et al.* developed a 3D porous PVDF/$Ti_3C_2T_x$ actuator for directional movement and controlled material transport in non-aqueous liquid systems using a solvent displacement method.[161] A foam was prepared by freeze-drying and the foam can be shaped using a template method. Upon IR light illumination, the actuator moves upward, and subsequent side illumination prompts horizontal movement, allowing it to cross the barrier in an oil-filled container. The actuator enables motion control and intelligent transportation in these artificial boats, allowing them to navigate, deliver materials, and transport loads with excellent motion flexibility.

When the ring of oxazine (OX) molecules opens, the zwitterionic form exhibits significant absorption in the visible light range because of its chromic properties and conjugated structure. Taking advantage of these characteristics of OX, Zheng *et al.* have designed an OX hydrogel actuator *via* a free radical copolymerization.[159] *N*,*N*′-Methylenebis(2-propenamide) (cross-linkers) and *N*-isopropyl acrylamide and oxazine (monomers) were dissolved in a mixed solvent consisting of *N*-methyl pyrrolidone/1,4-dioxane/water. *N*,*N*,*N*′- and *N*′-tetramethylethylenediamine (initiators) were subsequently added to the ammonium persulfate aqueous solution. Afterwards, it was put into certain molds, where it polymerized to create oxazine gels. Then the prepared gel was immersed sequentially in ethanol, *N*-methyl pyrrolidone and deionized water to obtain oxazine hydrogel. This oxazine hydrogel can be propelled on the water surface (Fig. 3g) and revealed excellent performance in obstacle avoidance, and cargo catching and transportation by a straightforward manipulation. The diameter, thickness and geometry of the hydrogel affects the speed of the actuator. The rotating motion of the hydrogel on the water surface is shown in Fig. 3h. The rotating speed of hydrogel actuator was controlled by both green and blue light.

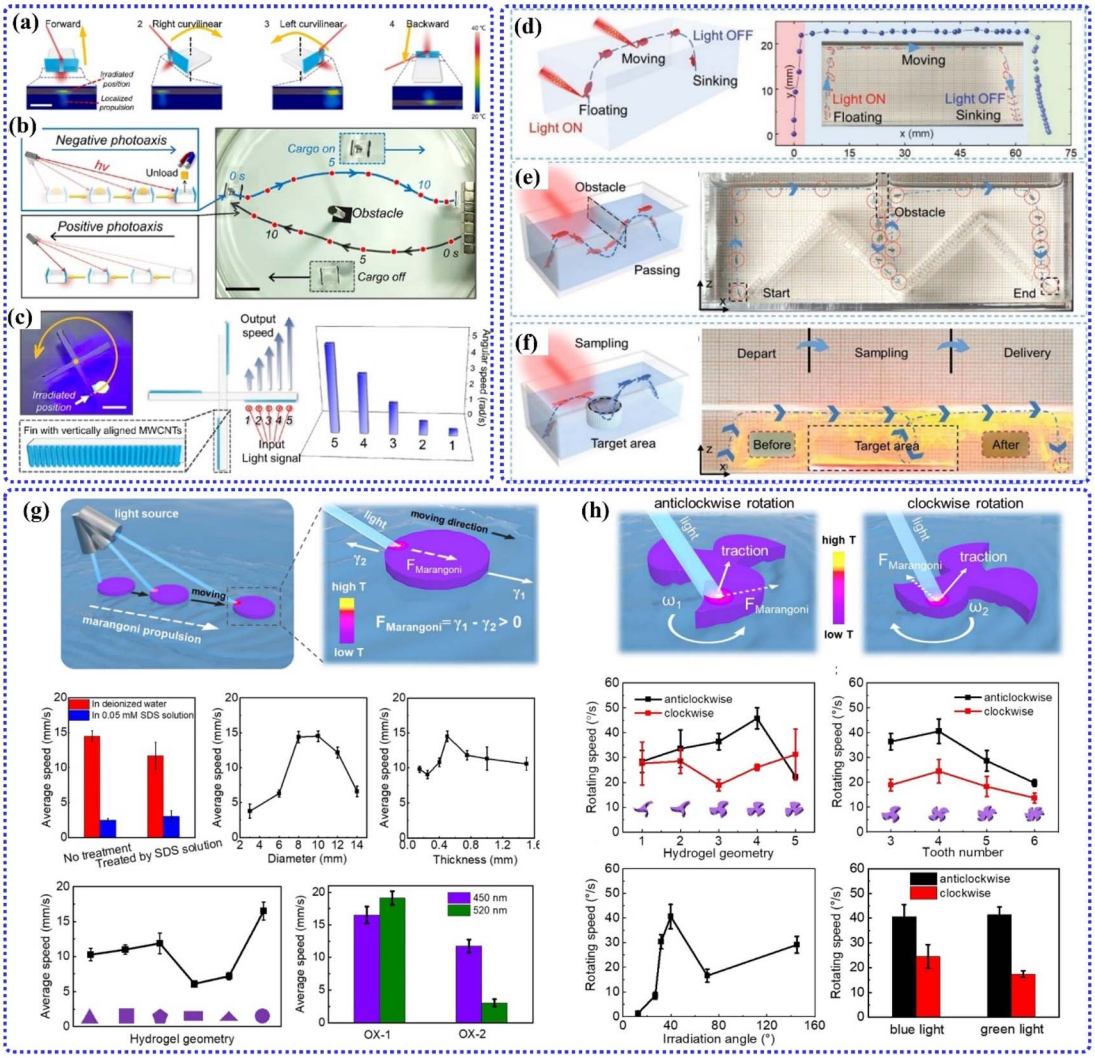

Fig. 3 (a) Schematic of light controlled moving motors. (b) Steering the boat through obstacles using light manipulation. (c) Photograph showing the angular rotation of the rotor. Reproduced from ref. 157 with permission from American Chemical Society, copyright 2018. (d) The diagram of the motion of LTMA in a liquid. (e and f) The obstacle avoiding, departing, sampling, and delivering processes of LTMA. Reproduced from ref. 158 with permission from Wiley-VCH GmbH, copyright 2021. (g) Schematic illustration of a light-fueled swimming of oxazine hydrogel and the swimming performance of oxazine hydrogel in water, as a function of different shapes of hydrogel, and average moving speed operated by blue and green light irradiation. (h) Schematic of the rotating motion of oxazine hydrogel, the rotating speed of hydrogels depends on its geometry, tooth number and irradiation angle and different colored light irradiation. Reproduced from ref. 159 with permission from Elsevier, copyright 2023.

The practical applications of photothermal materials with complex actuator configurations are significantly limited by the lack of nanotechnologies that allow for flexible integration. To overcome this challenge, by using direct laser writing technology, Wang *et al.* have created laser-induced graphene (LIG) tape, which can be applied to any surface to serve as a photothermal label for the development of photothermal actuators (Fig. 4a–c).[95] The swimming actuator was prepared by sticking a rectangular photothermal tape on a petiole of a leaf. The leaf could be driven in linear and rotational motion by blue laser light irradiation (Fig. 4d–g). Furthermore, the flexible photothermal tape folded in 3D origami acts as a 3D photothermal actuator and their translational and rotational motion could be controlled by light irradiation. Wang *et al.* developed floating gear actuators by incorporating CS into PDMS.[162] The SU-8 mold was created on a glass wafer using soft lithography. After that, CS was applied to the mold using a candle flame to form a 3D CS structure. PDMS was then used to enhance stability and create fluidic drag. It's important to note that the process differs for gear and pattern molds (Fig. 4h). The CS/PDMS actuators have high light absorption capacity in the 300 to 800 nm range and a power density of 2 W cm^{-2}. Their rotational, linear and curvilinear motions were controlled by IR light and focused sunlight. Fig. 4i shows different movement modes that were controlled by adjusting the irradiation position and their infrared images. The displacement and velocity of the actuator depends on the intensity of IR light (Fig. 4j and k). Fig. 4l and m show the clockwise and anticlockwise rotation of the actuator

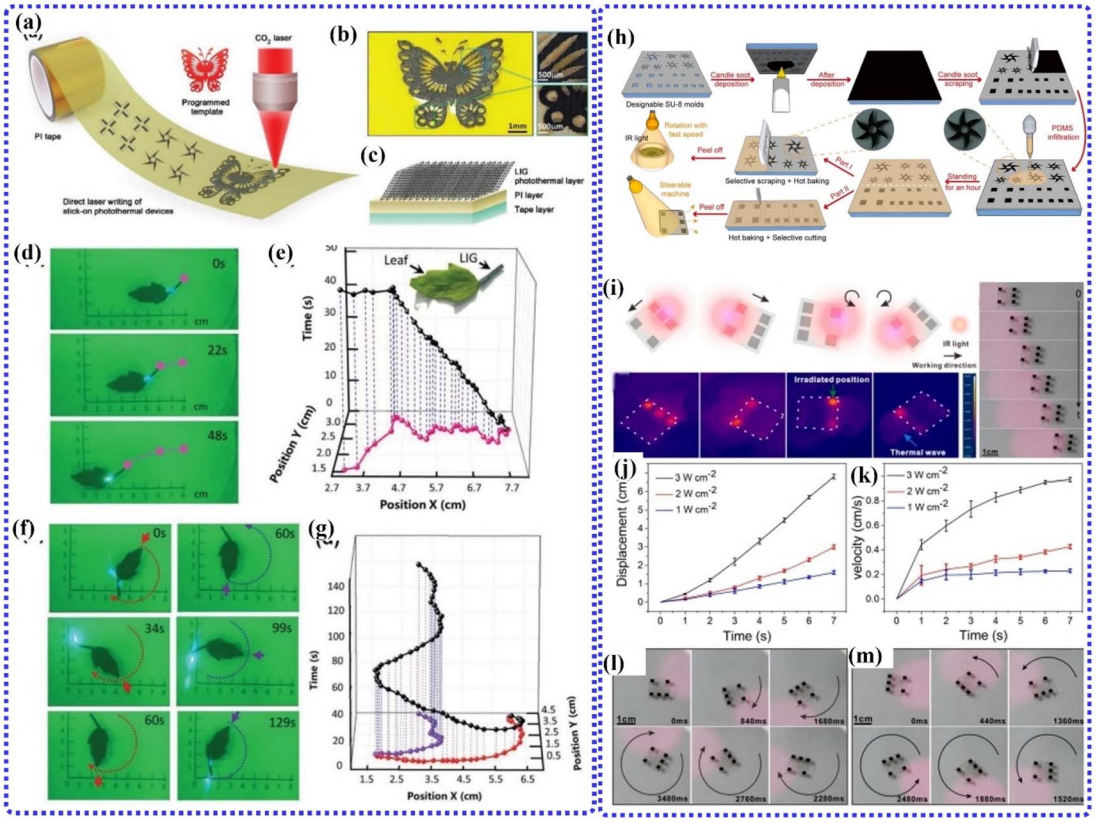

Fig. 4 (a and c) Diagram of the fabrication of LIG tape. (b) The image of LIG butterfly. (d and e) Directional and (f and g) rotation movement of the LIG leaf actuator. Reproduced from ref. 95 with permission from Wiley-VCH GmbH, copyright 2021. (h) Schematic of the fabrication of the CS/PDMS actuator and (i) the actuation performance of the CS/PDMS actuator. (j) The actual displacement and (k) the corresponding velocity of the actuator with time under changed IR light power. (l) Clockwise and (m) anticlockwise rotating motion. Reproduced from ref. 162 with permission from Elsevier, copyright 2021.

when light illuminated at one point of the actuator. Recently, Zhang *et al.* proposed the use of hollow glass microspheres (HGMPs) as carriers for low density photothermal conversion materials.[163] These HGMPs have excellent airtightness and low density. Further, HGMPs were modified with PDA to enhance their photothermal effect and surface functionality. PNIPAM was synthesized by loading with PDA-HGMPs. The lightweight PDA-HGMPs showed exceptional photothermal conversion efficiency. The actuators utilize buoyancy flow and the photothermal Marangoni effect to execute floating, descending, and swimming movements. The laser modulates the actuator's motion by adjusting its switching state throughout different stages of motion. Integrating sensors within these actuators is vital for the advancement of intelligent soft robots.

However, the Marangoni effect only works on objects floating on liquid/liquid and liquid/air interfaces, limiting its further development and application. To address this challenge, actuators were assisted by bubbles/vapors that can provide sufficient vertical propulsion force for actuators leading to multi-direction aquatic motion.[164] Luan *et al.* have successfully developed a photothermally responsive actuator capable of various controllable motions in an underwater environment.[165] For the horizontal motion, the motor utilizes oxidized copper foam (OCF) and PDMS-coated oxidized copper foam (POCF). The POCF traps air bubbles during immersion into water. When illuminated by laser light (532 nm), the trapped air bubbles expand, increasing the buoyancy of the POCF motor and causing it to revolve counterclockwise around one side. Turning off the light results in the shrinkage of bubbles due to rapid heat dissipation, leading to horizontal motion. For vertical motion, a different design is employed that incorporates a porous, hydrophobic PDMS foam doped with carbon black and a magnet. Similar to the horizontal motion, the volume of air bubbles can be adjusted to regulate the apparent density of the C-foam actuator and achieve vertical motion.

3.2. Expansion/contraction

Bionic crawling-like robotic movement can be achieved by self-contraction/expansion under light illumination. The layered photothermal materials (lower and larger CTE layers) produce bending deformation under light irradiation. For example, a CNT embedded PDMS film reveals reversible bending under NIR irradiation.[166,167] As the temperature increases, PDMS expands, while CNTs remain relatively stable and cause deformation and bending towards the CNT side. The bending endorses mechanical strength and achieves actuation. Deng *et al.* have developed a visible-light-driven actuator by spin-

coating of melted paraffin wax onto a Kapton film, followed by layers of aligned CNTs.[80] The paraffin wax/CNT composite layer and Kapton film were compactly contacted, improving heat transfer and mechanical coherence. The nanoscale gaps between the aligned CNTs were filled with wax, resulting in a structure resembling plant cell wall. Strips A and B were prepared by transversely and longitudinally aligned CNTs on Kapton film. This actuator emulates a pine cone's reversible open and close action. As the temperature increased by the photothermal effect of CNTs, the composite film stretched along the transverse direction. Additionally, different thermal diffusion rates caused the edges to extend less than the middle area, resulting in a contractile stress appearing in the longitudinal direction. Therefore, strip A exhibited apheliotropic bending, while strip B showed phototropic bending under light irradiation. The plant like moment of the actuator is shown schematically in Fig. 5a. Wang and colleagues prepared a hydrogel bilayer actuator by combining an active layer of PNIPAM with a PDA-modified P-MXene and calcium chloride ($CaCl_2$) composite hydrogel, and a passive layer of acrylic acid (AA) and amphoteric [2-(methacryloyloxy)ethyl]dimethyl-(3-sulfopropyl) (SBMA).[168] A strong interfacial bond formed by coordination of carboxylate and Ca^{2+}. The remarkable adhesion capability of the PAA/SBMA layer to PNIPAM (280 N m^{-1}) and high light response to bending enable a smart adhesion actuator to be designed for the mechanical gripper. P-MXene demonstrates exceptional photothermal properties, causing the actuator to bend nearly 360° in 10 s by NIR irradiation. The smart actuator can grasp, transfer, and release irregular shaped objects for example sponge and glass bottles as shown in Fig. 5b and c. Due to its temperature dependent adhesive properties, the actuator can lift objects at high temperature and release them at room temperature as shown in Fig. 5d and e.

Similarly, Li *et al.* have designed a bilayer actuator by a photothermally sensitive hydrogel layer and PDMS layer.[61] The hydrogel was created by the thermally sensitive hydrogel PNIPAM with hydroxyethyl methacrylate (HEMA) and GO as photothermal materials. The HEMA effectively drives water molecules inside the hydrogel, which causes bending. Upon exposure to xenon lamp irradiation, the actuator undergoes bending as a result of shrinkage in the hydrogel and expansion in the PDMS. As shown in Fig. 5f(i) and (ii), the actuator bends the hydrogel side under xenon lamp irradiation. A Y-shaped actuator gradually bends the upper part under photothermal radiation (Fig. 5g). The bending angle increases with longer laser irradiation time. The actuator has independent driving capabilities and is able to grasp a target ball, resembling the mechanical claws of a pinball machine (Fig. 5h). A cross shaped actuator transports the ball vertically downward through thermal response deformation (Fig. 5i).

In cold environments, the photothermally induced heat energy is dispersed into the surrounding environment, which can cause a decrease in actuation performance and limit the applications of the technology. To combat this issue, Li *et al.* have developed a hydrogel actuator with thermal dissipation resistance.[169] This actuator is made up of vulcanized layered double hydroxide (VLDH) nanosheets combined with PNIPAM and implanted on poly(acrylamide) (PAM) hydrogel (Fig. 6a). The

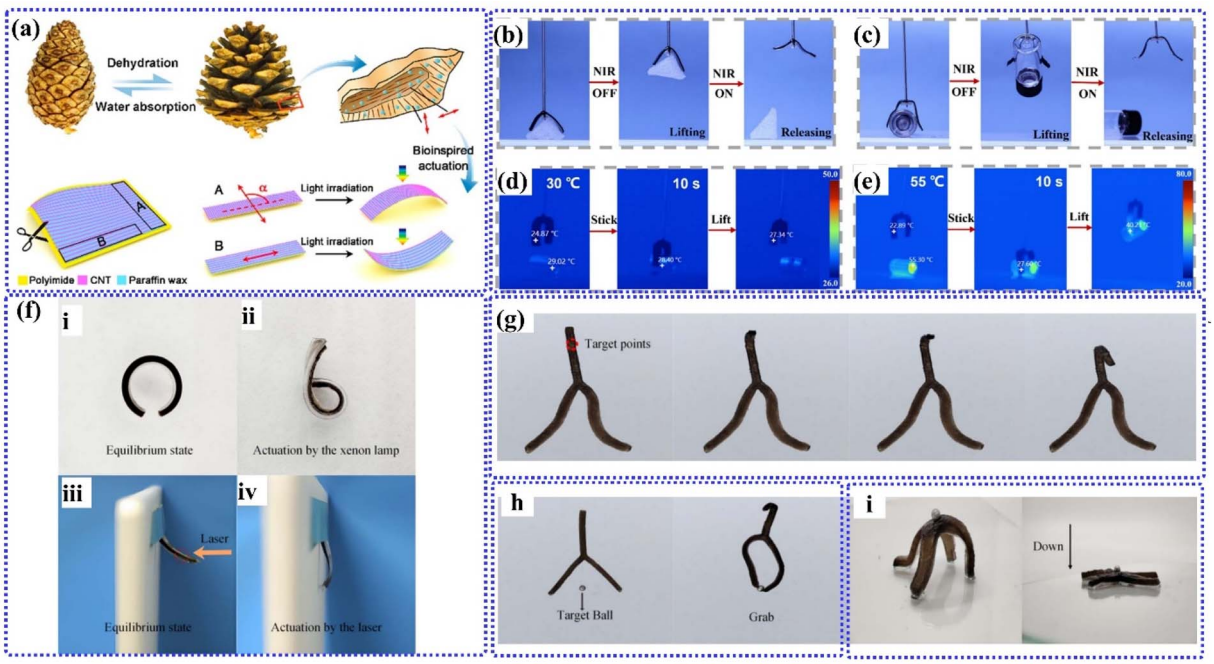

Fig. 5 (a) Pine cone like opening and closing movements of CNT composite strips. Reproduced from ref. 80 with permission from American Chemical Society, copyright 2016. (b–e) The object lifting and releasing behavior of hydrogel actuators by photothermal actuation. Reproduced from ref. 168 with permission from American Chemical Society, copyright 2023. (f) Photographs of the photothermal bilayer actuator made of PGH/PDMS showing the change in bending (i–iv). (g–i) The differently shaped actuator behaves independently to capture and transport a target ball. Reproduced from ref. 61 with permission from Royal Society of Chemistry, copyright 2023.

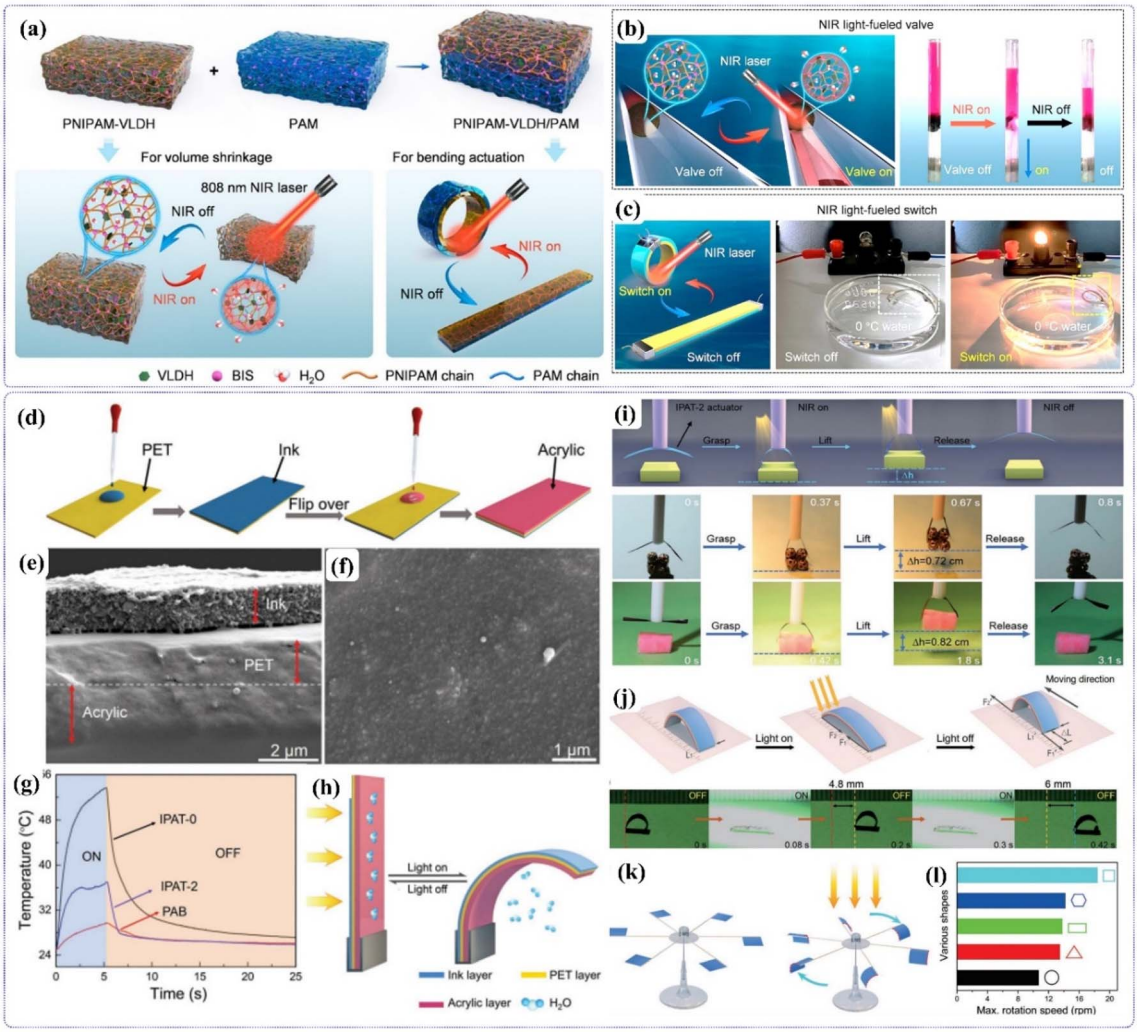

Fig. 6 (a) Fabrication process of bilayer hydrogel actuators, and their volume shrinkage and anisotropic bending. Photographs of (b) liquid valves and (c) a switch fabricated from the bilayer hydrogel. Reproduced from ref. 169 with permission from American Chemical Society, copyright 2023. (d) Schematic of the IPAT actuator fabrication process. (e and f) SEM image of the IPAT and the ink surface. (g) Variation of temperature with time of actuators under NIR irradiation. (h) Schematic of performance of the photothermal actuator. Schematics and photographs of (i) grabbing an object, (j) a walking robot and (k) light mill. (l) The correlation between the shape of the actuator and the rotational velocity of the light-powered mill. Reproduced from ref. 170 with permission from WILEY-VCH Verlag GmbH & Co. KGaA, Weinheim, copyright 2019.

hydrogel actuator (PNIPAM-VLDH) shows similar photothermal performance even at temperatures lower than 0 °C compared to 25 °C. Below −5 °C, the generated temperature decreases due to excessively low temperature. The hydrogel demonstrates a significant 46% volume reduction upon exposure to NIR light at 808 nm and 660 mW cm^{-2}. This effect is attributed to the selective shrinkage of the PNIPAM layer, while the PAM layer remains unchanged. The volume shrinkage of the PNIPAM-VLDH hydrogel and bending of bilayer PNIPAM-VLDH/PAM hydrogels are shown in Fig. 6a. This hydrogel was used as a valve to control fluid flow in a cold environment. Fig. 6b illustrates red rhodamine B solution and air separated by the hydrogel inside the quartz tube. For fabricating a bilayer actuator, the PNIPAM-VLDH hydrogel grafted onto PAM exhibited bending under NIR irradiation. Such bending actuators can be used in electronic switches which operate in a cold environment (Fig. 6c).

In conventional bilayer photothermal actuators, the response time, bending speed, and bending amplitude of actuators can be enhanced by adjusting the CTE difference, intensity/wavelength of light, and thickness of active and passive layers. Further, tri-layered photothermal actuators were designed with a cooling layer in addition to active and passive layers of bilayer actuators that improves actuation performance through volume reduction caused by water evaporation. Li *et al.* prepared a tri-layered photothermal actuator that consists of an ink layer, PET film, and an acrylic adhesive layer (Fig. 6d).[170] The ink was made using a mixture of carbon black and polyurethane and then spin-coated onto PET. The acrylic adhesive layer was also spin-coated on PET to create a tri-layer actuator (IPAT). The layers are designed to absorb light, convert it to heat, and produce water desorption upon heating. This results in decreased film temperature and increased bending amplitude

of the actuator. The cross-sectional microscopic image reveals the layered composition of the actuator (Fig. 6e) and carbon black deposited ink surface (Fig. 6f). Due to photothermal heating, the acrylic adhesive evaporates adsorbed water molecule and hence consequently shrinks in volume. Fig. 6g illustrates variation of temperature with time of light irradiation. Due to the large CTE difference between the carbon black slurry and PET, the actuator bends towards the PET side (Fig. 6h). The reduced volume acrylic adhesive and their negative value of CTE eventually enhances the bending of the actuator. Such tri-layer actuator exhibited fast response and high bending speed (72.5° s^{-1}) under NIR light. By taking advantage of these properties, authors have demonstrated a light mill, soft crawling and mechanical gripper (see Fig. 6i–l).

Recently, Gu *et al.* have developed a tri-layered soft actuator using a PDMS/graphene/mica membrane.[171] Fabrication involved the following steps. Poly(vinyl alcohol) (PVA) was spin-coated on a glass substrate. A muscovite mica film was placed on top, then graphene dispersion was added. PDMS was spin-coated on the graphene film. After curing, the PVA was dissolved in water, resulting in a freestanding PDMS/graphene/mica film. The actuator achieves a curvature change of approximately 0.6 mm in 7 s under 150 mW cm^{-2} of illumination intensity of light and can carry payloads over 18 times its own weight. These photothermal actuators exhibit quick, reversible, and adjustable bending movements at specific locations; the remarkable results highlight the ability of photothermal expansion and contraction to enhance actuation, paving the way for groundbreaking advancements in high-performance photothermal actuators.

3.3. Phase transition

To achieve light-responsive phase transition, LCPs and SMPs are combined with photothermal materials. Once photothermal materials generate heat under light irradiation, LCPs exhibit isotropic phase transition. The LCPs contract along the mesogens, but expand in their vertical direction. For example, Yang *et al.* have reported that single-walled CNT loaded LCE contracted 80% under light illumination.[172] Liu *et al.* have fabricated a photothermal actuator using gold nanospheres and gold nanorods as LCE micropillars.[173] The gold nanomaterials generated localized heat under light illumination through the plasmon resonance effect. Gold nanorods exhibited better photothermal performance than gold nanospheres. The photothermal actuation performance of the LCE/gold nanorod micropillar actuator was evaluated in silicon oil. When a laser beam is directed at a micropillar, the micropillar undergoes a reduction in length and then swiftly expands its diameter within a span of 5 s. Upon cessation of the laser light, the micropillar promptly returns to its original form within 1.5 s.

To overcome the issue of dissolving the photosensitive inorganic materials into the organic polymer, Li *et al.* have directly dispersed organic photothermal PDA particles into the LCE.[174] The PDA–LCE composite was sandwiched between two glass slides and dried at 180 °C for 4 h. Subsequently, the resultant film was trimmed to produce a different actuator shape. PDA contains many amino and hydroxyl groups, it has strong light absorption, excellent photostability, and high efficiency in converting light to heat. The temperature of the LCE increased to 160 °C within 15 s, resulting in reversible actuation as the light was turned on and off. Tian *et al.* have created an optically responsive elastomer film by utilizing a PDA-coated LCE, which is capable of functioning in both air and water.[175] The process for fabricating PDA-coated LCE films is simple and versatile, involving molding, pre-stretching, and dip-coating.

Under NIR irradiation, the LCE contracted within 1/10 s. The PDA coated LCE bends or rolls on the surface and swims on water by NIR laser light. One end of the PDA-coated LCE film was fastened, while the other end was kept free for the purpose of studying bending deformation. When the free end of the film is exposed to NIR light, it may rise 22.5 mm in 0.17 s and return to its initial position in 0.48 s (Fig. 7a). As the NIR light scans the film from bottom to top, the film can be rolled up (Fig. 7b). The film contracted as it was scanned from bottom to top. This contraction under NIR light irradiation was utilized to easily lift an object (Fig. 7c). By considering reversible bending and unbending under on/off of NIR light, a macroscopic prototype of the robotic swimmer was designed, as shown in Fig. 7d. After exposure to NIR light the surface of the LCE (tail of the swimmer) bent and quickly recovered its original stage (unbent). This bending and unbending of the LCE surface on water exerts a force on the water surface, resulting in dynamic motion of the swimmer on the water surface (Fig. 7e). Fig. 7f shows snapshots of the forward motion of the swimmer and displacement with respect to time. Due to lower percentage of solubility of photothermal materials in the organic polymer, photothermal actuators exhibited poor actuation/bending performance. Liu *et al.* have chemically bonded the LCE polymer chain with a chromophore crosslinker, which absorbed NIR light and exhibited excellent mechanical deformation.[176] Under NIR stimulation, the temperature of LCE increased to 260 °C in 8 s and exhibited contraction and expansion while light was turned off. Recently azobenzene chromophore crosslinkers as photothermal agents have been used with organic polymer actuators.[177,178]

Moreover, SMPs can be used as a shape deformation layer for the photothermal actuator. SMPs such as PNIPAM can contract their shape at temperatures higher than their lower critical solution temperature. Therefore, in combination with photothermal materials, the temperature of SMPs increases under light irradiation. Based on this principle, Chen *et al.* have combined GO–PNIPAM/GO for an actuator, in which heat transferred to the GO–PNIPAM layer causes bending performance in the PNIPAM layer direction.[56] Like phase transition induced volume change deformation, molecule adsorption and desorption exhibit large volume change. As temperature increases, hydrophilic PDA and PNIPAM evaporate water molecules, causing a decrease in volume. Based on the temperature dependent evaporation of water molecules, photothermal actuators are smartly combined with these soft materials. The power of phase change processes lies in their ability to store and release immense amounts of energy, which can be harnessed to drive actuators. Very recently, Han and

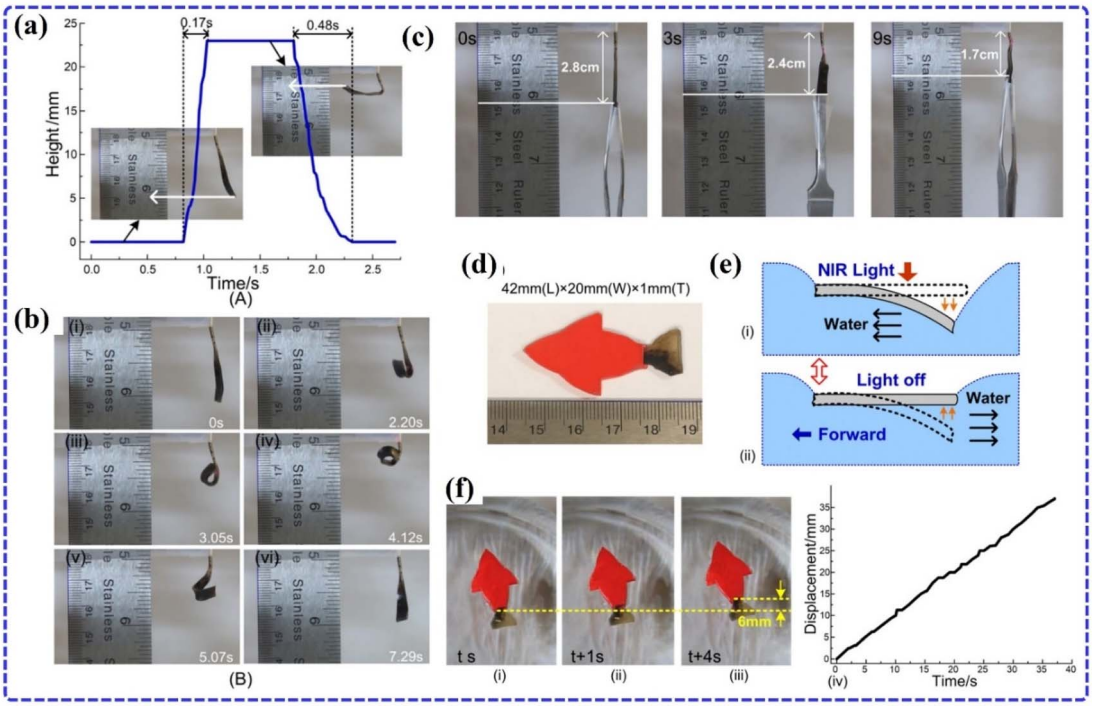

Fig. 7 (a) Deflection, (b) rolling, and (c) object lifting performance of the PDA–LCE film under laser irradiation. (d) Photograph of the robotic swimmer. (e) The bending (i)/unbending (ii) of the fish's tail fin. (f) Measurement of the swimming performance of the soft robotic swimmer. Reproduced from ref. 175 with permission from American Chemical Society, copyright 2018.

colleagues have developed a bilayer hydrogel actuator that utilizes tannic acid–gelatin (TAG) shape memory hydrogels, Fe_3O_4 nanoparticles, and gelatin–polyacrylamide (GAM) hydrogels.[179] When the TAG layer is subjected to heat or NIR light, it returns to its original state, causing a change in shape. When exposed to NIR irradiation (2.5 W cm^{-2}), the TAG–Fe_3O_4 layer undergoes contraction, leading to the hydrogel bending into a circular shape within 50 s. Taking these advantages the different forms of soft robots were created. TAG–Fe_3O_4 hydrogels assembled on fingers can rapidly bend under NIR, and arms of a hydrogel athlete can lift a barbell. Similarly, hydrogel athletes can simulate exercises such as front levers and crunches.

4. Superhydrophobic photothermal actuators

There are still some challenges when it comes to using photothermal actuators in practical applications. For instance, when driving on the water surface, certain factors such as bacterial growth, corrosion, organic contamination, and high drag force can affect the performance of photothermal actuators.[50,110] The water opposes the flow of poor hydrophobic photothermal actuators because of the partial attraction between water and the actuator surface. It also possesses lower weight-bearing capability. To overcome these challenges, the superhydrophobic modification has remarkable functional characteristics that reveal the ability to float on the water surface, drag reduction,[180,181] self-cleaning,[182,183] anti-corrosion,[184,185] oil spill recovery[186–188] and high-speed self-actuation.[189,190] The surface energy and roughness contribute to attaining surface superhydrophobicity.[60,191] Floating objects are propelled by a surface tension differential created by temperature. Due to the superhydrophobicity, a thin air layer formed underneath the photothermal actuator, which causes drag reduction during the motion and also improves weight-bearing capacity. Such actuators are promisingly used in micro-robots, environmental remediation, bioengineering, smart transportation, contactless delivery, and oil spill recovery.

The synergistic superhydrophobicity and photothermal effect to develop non-contact propulsion in an aquatic environment is a remarkable breakthrough that inspires innovation. Chen *et al.* have prepared a photoresponsive actuator based on a bilayer composite of graphene/PDMS and PDMS layers.[52] As shown in Fig. 8a, a mixture of PDMS, curing agent, and graphene was stirred magnetically and added to *n*-hexane in preparation. After the ultrasonication, the mixture was applied onto a glass substrate. The composite was then dried under a vacuum to form a uniform layer of graphene/PDMS. A bilayer actuator was prepared by applying the mixture of PDMS and curing agent on to the graphene/PDMS film. It was then cured at 100 °C for 2 h in a vacuum drier. The aquatic robot was designed by laser cutting of bilayer film. The introduction of graphene in polymers improves the hydrophobicity of the bilayer film, and further addition of the graphene film exhibited a water contact angle (WCA) greater than 120°. The graphene network constructed PDMS composite bilayer film displayed excellent photothermal conversion ability. The surface

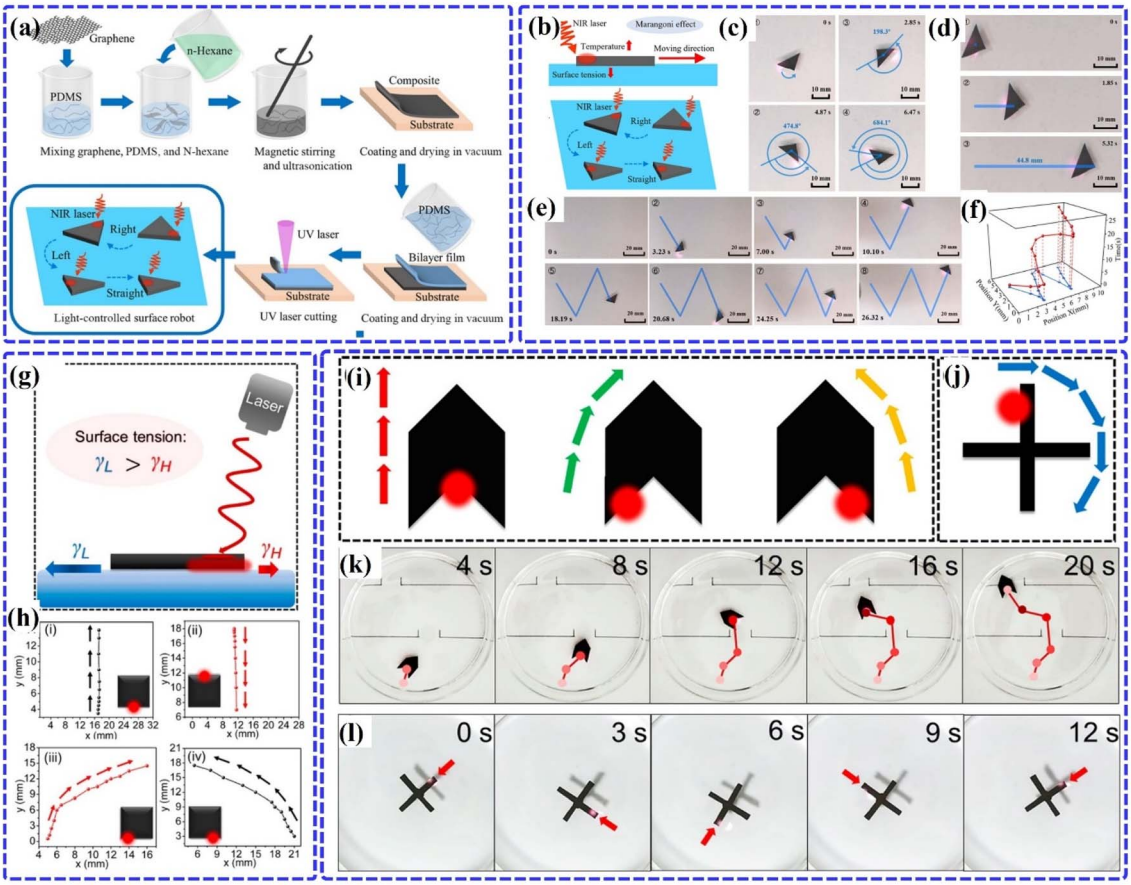

Fig. 8 Schematic for (a) fabricating the graphene/PDMS actuators and (b) actuation of the robot on the liquid surface. (c–f) Photographs of a robot in rotary, linear, trajectory and "W" shape motion on the liquid surface. Reproduced from ref. 52 with permission from American Chemical Society, copyright 2023. (g) Schematic of the Marangoni flow under light. (h) Moving pathways of the HN–PDA–OA paper actuator. (i–l) The different shaped HN–PDA–OA paper actuators and their different moving directions. Reproduced from ref. 192 with permission from American Chemical Society, copyright 2019.

temperature increases with concentration of graphene and laser light power. For 30% of the mass fraction of graphene, the surface temperature rose to 120 °C within 1 s at 4.4 W cm^{-2} of infrared laser irradiation power. A triangular-shaped microrobot was driven by a NIR laser on a fixed path (Fig. 8b–d). Such microrobot moves straight on the water surface at 8.42 mm s^{-1} and a rotating speed of 106° s^{-1}. Moreover, it achieves complex 'W' trajectory propulsion (Fig. 8e and f).

Wu *et al.* have applied a layer of fluorinated acidified carbon nanotubes (F-ACNTs) onto filter paper, followed by a Fe_2O_3/PDMS mixture layer to create a superhydrophobic photothermal actuator.[193] Surface roughness and wettability are significantly influenced by the Fe_2O_3 with PDMS proportion. At a weight ratio of 3 : 2, the coating exhibited a high WCA of 157.4° and sliding angle (SA) of 3°. The presence of the CNT material in the layer possesses excellent photothermal conversion performance, reaching a surface temperature of 130 °C within 30 s under NIR light illumination. A layer of air is created between the water surface and the superhydrophobic coated paper, allowing it to float on the water with reducing resistance of water when in motion. While the coated paper converts absorbed NIR light into heat, it heats the water and produces a surface tension gradient, which propels the coated paper on the water surface in the horizontal direction. In another study, Yang *et al.* have created flexible, superhydrophobic, and photothermal paper by coating a composite of PDA, hydroxyapatite nanowires (HNs) and oleylamine (OA).[192] The HN–PDA–OA paper demonstrated different directional motion under light irradiation because of its superior photothermal conversion and superhydrophobic properties (Fig. 8g and h). The HN–PDA–OA paper can sustain loads up to 80 times its own weight and it is driven with a velocity of 5.05 ± 1.62 mm s^{-1} under NIR light. The designed arrow-shaped and cross-shaped actuator shows excellent self-propulsion under NIR light illumination (Fig. 8i–l). Chen *et al.* have used Fe_3O_4, CNT, and methyltrimethoxysilane (MTMS) to create a sandwich-like structure on a wooden surface.[194] The *in situ* co-precipitated Fe_3O_4 and spray-deposited CNT work synergistically to convert light into heat, while the vapor deposition of MTMS generates a superhydrophobic surface. Modified wood exhibits a static WCA of 151° and repels both acidic and alkaline solutions. The superhydrophobic photothermal wood moves forward straight when exposed to NIR and sunlight due to reduced drag and variable surface tension.

Table 2 Comparative study of superhydrophobic photothermal actuators

Materials	Laser light intensity [W cm^{-2}]	Velocity of the actuator [mm s^{-1}]	Response time [s]	Contact angle [°]	References
F–ACNTs/Fe_3O_4 and/PDMS	1.5	8.9	1.9	157.4	192
ACNTs/Fe_3O_4/ODA/PDMS	1.5	—	—	161	197
ODA–(MWCNTs–COOH/MWCNTsNH$_2$)$_6$	2	—	30	165	198
HN–PDA–OA, paper	1.0	3.8	2.2	154.1	192
HN–Ti_2O_3–PDMS, paper	1.0	4.3	1.4	151.2	199
CNF, FAS	0.9	4.6	1.3	153.6	195
MXenes–FAS, paper	1.0	7.9	1.5	163.1	144
TiN–PDMS–PVDF papers	1.5	10.1	0.8	169.9	34
Graphene–PDMS	3.4	7.5	—	161.8	200
PDMS@MS/MoS_2	0.6	8.27	—	158.5	201

Due to the high light absorption and photothermal conversion ability of MXene, Cao and colleagues applied a spray coating technique on fabric, paper, and glass substrates to create a superhydrophobic surface using a composite solution of hydrophobic multi-layered MXenes, delaminated MXenes and PDMS.[144] The hydrophilic MXenes were modified by fluorinated alkyl silane (FAS) for hydrophobicity. The surface analysis confirms that micro-sized multi-layered MXenes and nano-sized delaminated MXenes created micro/nanoscale roughness. Such surface has shown superhydrophobicity with a WCA of 163.1° and SA of 8.7°. The spray-coated paper was trimmed into a triangular shape to analyze controllable actuating on the water surface under NIR laser illumination. The linear and rotation motion is achieved by irradiating the specific location of the coated paper. Rotational motion was created when NIR light was applied to one side of the triangular-coated paper. Also, it demonstrated that the light-induced pressure (2.6×10^{-9} N) is significantly less than the gravity of the paper (1.4×10^{-4} N).

In most of the work, lightweight polymer substrates have been used to fabricate photothermal actuators or polymer adhesives to improve interfacial adhesion. However, polymers possess low thermal conductivity. In photothermal conversion, a large amount of localized heat can be generated, which causes the failure of interfacial adhesion due to the low thermal conductivity of the polymer adhesive and sometimes igniting the polymer substrate, failing actuation. To address this issue, Song *et al.* have used the electrospinning method to fabricate a multi-responsive superhydrophobic carbon nanofiber membrane.[195] The membrane was created using a composite solution of polyacrylonitrile and nickel acetylacetonate, which was then heated and fluorinated. In the first step, the membrane is heated in air at 240 °C for 2 h. Then, it is carbonized by heating it at 900 °C under N_2 and modified by FAS. It revealed outstanding photothermal performance, and triangular-shaped carbon nanofibers were irradiated with a 0.9 W cm^{-2} NIR laser. The membrane moved in clockwise and anticlockwise rotation with 1.05 rad s^{-1}. Due to wetting, the unfluorinated nanofiber failed to drive on the water surface under the same illumination. In another study, Fan *et al.* recently created superhydrophobic light-driven actuators by growing copper sulfide (CuS) on cellulose nanofibers (CNF) and then modifying them with octadecyltrimethoxysilane (OTMS).[196] These actuators demonstrated exceptional superhydrophobicity with a WCA of 160.6° and exhibited a temperature of 81.0 °C when exposed to NIR irradiation at 808 nm and 1.4 W cm^{-2}. The actuators demonstrate linear, rotation and intricate motion when subjected to a single stimulus, resulting in distinct moving patterns. Additionally, it is capable of carrying payloads and absorbing oil, making them valuable for urgent environmental cleanup efforts. The comparative performance of superhydrophobic photothermal actuators is illustrated in Table 2.

5. Applications of photothermal actuators

Photothermal actuators have potential applications in various fields, including micro-robots, environmental remediation, bioengineering, transportation, wireless delivery, and oil spill recovery due to their actuation controlled by light. Photothermal actuators have been designed based on the surface tension gradient, phase transition, and contraction/expansion for various applications. This section discusses the utilization of photothermal actuators across various applications.

5.1. Bionic robots

Every robot has unique characteristics and actuating performance, making them suitable for various applications. Chen *et al.* have prepared bionic robots using thermal-regulated graphene/PDMS and PDMS bilayer film.[52] As shown in Fig. 9a–c, the flower curled and closed at room temperature, when laser light irradiated the bionic flower it gradually opens. It could cool rapidly when the laser light is switched off because the composite material has a strong heat conductivity. A caterpillar-like bionic crawling robot was created by connecting two bilayer thin films in an inverse manner. The crawling of the robot is shown in Fig. 9d and e. When laser light is irradiated, the bending angle varies, which causes propulsion in the forward direction.

Similarly, another literature presented a bionic water strider-like crawling robot.[202] Superhydrophobic feet and a superhydrophobic body were attached to opposite sides of the actuator to create the legged water-walking soft robot shown in

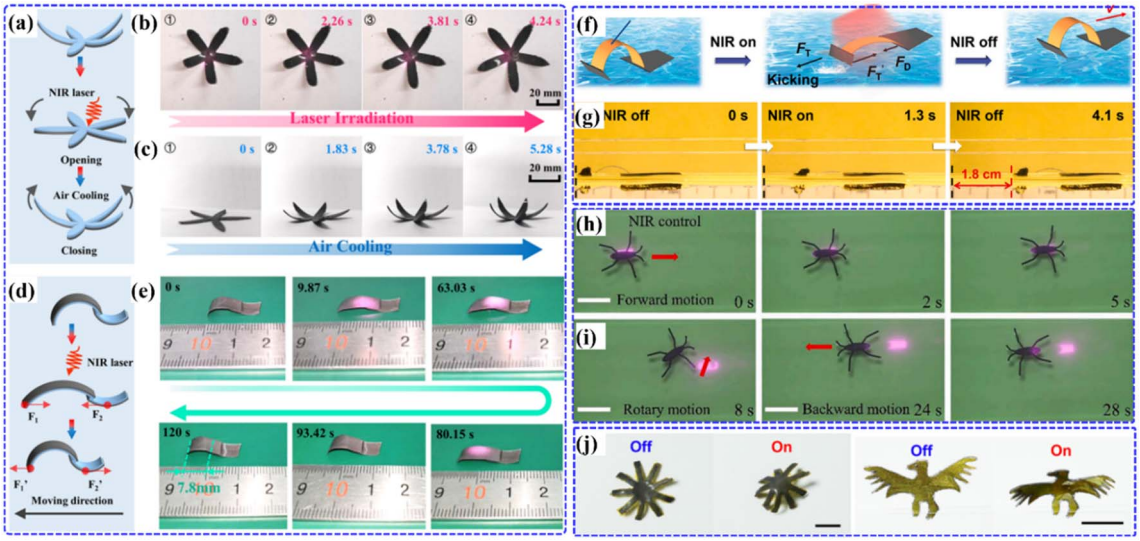

Fig. 9 Bionic-like crawling robot, (a–c) schematic of actuation, and optical images of the actuation mechanism of the bionic flower. (d and e) Caterpillar-like robot crawling mechanism. Reproduced from ref. 52 with permission from American Chemical Society, copyright 2023. (f) Schematic of the aquatic soft robot. (g) Image of a water walking one-legged soft robot. Reproduced from ref. 202 with permission from Elsevier, copyright 2022. (h and i) The water strider robot realizes different direction of motion under the infrared laser. Reproduced from ref. 200 with permission from Elsevier, copyright 2021. (j) Morphing of spider-inspired and eagle-inspired soft robots. Reproduced from ref. 203 with permission from Springer Nature, copyright 2023.

Fig. 9f and g. The actuator bends under laser light and generates a backward thrust force (FT) on the water due to the foot. The robot water walks like a water strider due to the high reactive force from the water compared to the drag force (FD). Water walking stopped when the NIR light was removed and resumed with photoirradiation due to FD. The aquatic soft robot propels itself by repeatedly kicking while the NIR light is turned on and off. Wang *et al.* prepared photoresponsive superhydrophobic microrobots using a composite of graphene and PDMS without any further chemical modifications.[200] This graphene/PDMS composite material has self-cleaning, oil recovery, light-driven actuation, and water-strider-like walking robot properties. The superhydrophobic composite contains numerous micro and nano-pores, allowing oil droplet absorption and water repelling. The composite of graphene and PDMS possesses remarkable photothermal properties that enable it to propel microrobots on the water surface. The microrobot reveals both directions of movement away from the light source and toward the light. The microrobot's velocity increases with the light's intensity, increasing the temperature and exerting a force on the microrobot due to the surface tension difference of the liquid. A graphene/PDMS composite was used to prepare a water strider like robot that moves on water (Fig. 9h and i). The robot moved at a speed of 5.4 mm s^{-1} on the water surface under the influence of laser light. The photoresponsive superhydrophobic graphene/PDMS based microrobots were used for detection or oil recovery. The WSe_2 and graphene-introduced PDMS layer revealed photothermal actuation.[203] The spider and eagle-shaped soft robot exhibited propulsion under laser irradiation (Fig. 9j). The spider robot's claws and body retract inward, enabling curling. The eagle wings flap inward and imitate the flying behavior under laser irradiation.

5.2. Aquatic robot

With the growing demand for contactless and light-driven actuators, many efforts have successfully employed photothermal actuators in various fields, including oil recovery, contactless transportation and cargo delivery, and power generation, summarized in Fig. 10. Ning *et al.* have developed a lightweight, 3D, light-driven actuator for driving and swimming on the water surface using PVDF/graphene nanosheet (GNS) foam, made up of a melt blend and hydrophobic modification.[98] For the fabrication of the actuator, first the composite of PVDF, GNS, and sodium sulfate (Na_2SO_4) was sequentially melted and blended.

The composite sheet made of PVDF, GNS, and Na_2SO_4 was ultrasonicated in deionized water, causing the Na_2SO_4 to be removed and resulting in the PVDF/GNS foam. The foam was then modified with FAS-17 in a second step to achieve superhydrophobicity. Under NIR laser irradiation, the foam actuator propulsion in water is faster than in acid, alkali, and salt. The oil stain was successfully removed by the superhydrophobic photothermal foam actuator moving by light (Fig. 10a). As shown in Fig. 10b and c, the graphene-based navigated boat is driven by light for *in situ* navigating in narrow terrains.[204] The wireless, contactless, and light-driven robot boat has promising transportation and in-pipe inspection applications. The microstructure created by square pillar arrays underneath the boat could enhance the loading capacity by 12.75% and moving speed by 16.7% compared to that without a microstructure. The loading capacity of the robot was 2.24%, and its movement response along the grating lines was 34.65%. Hou *et al.* designed light-driven ships for smart transportation and contactless delivery (Fig. 10d).[101] Such a boat can carry twice the

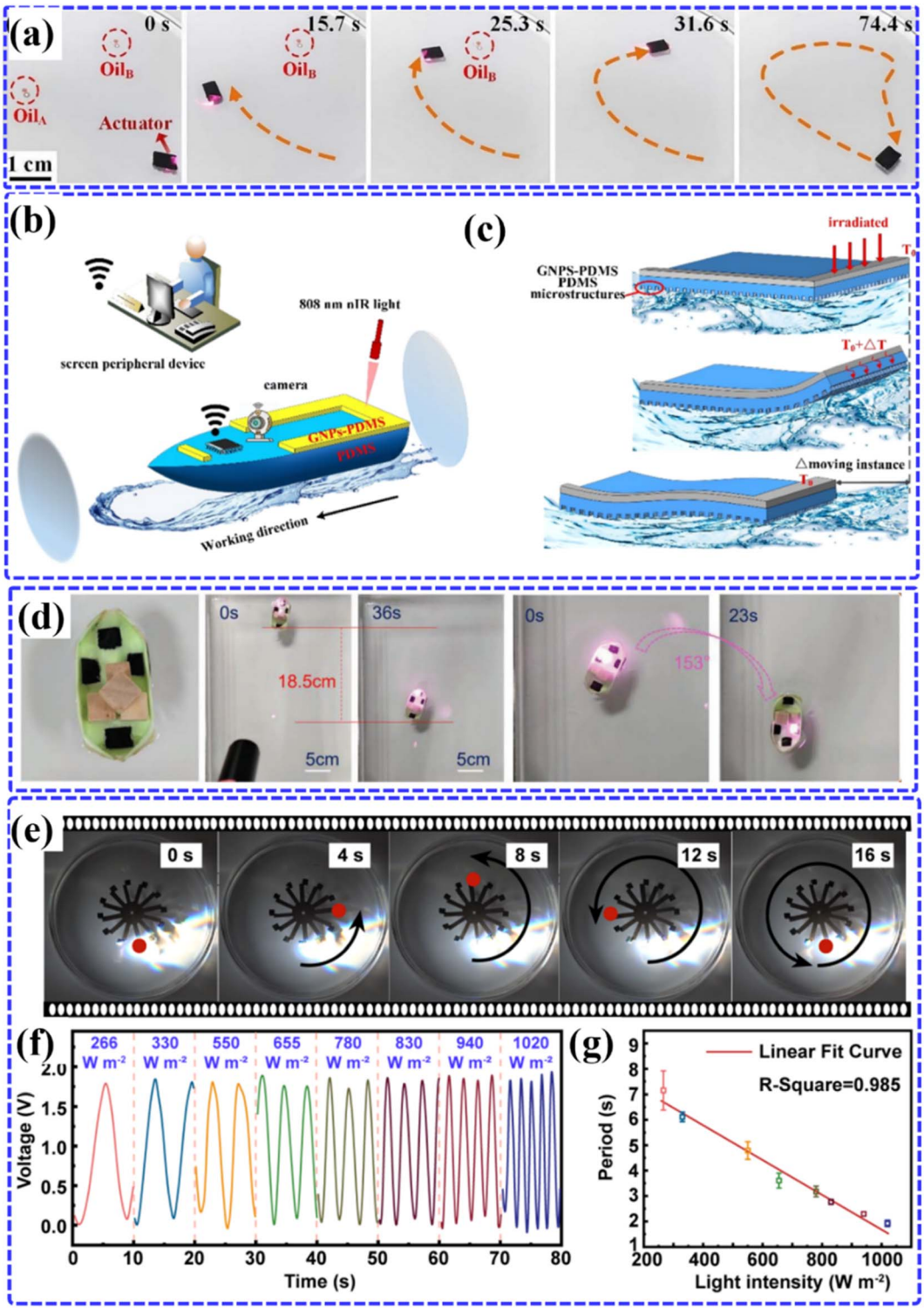

Fig. 10 (a) Image of the oil absorption process of actuators. Reproduced from ref. 98 with permission from Elsevier, copyright 2023. Diagram of the wireless soft robot boat monitoring. (b and c) Mechanism of the light-driven robot boat. Reproduced from ref. 204 with permission from American Chemical Society, copyright 2020. (d) Image of the light-driven ship carrying cargo. Reproduced from ref. 101 with permission from Wiley-VCH GmbH, copyright 2023. (e) Sunlight-induced rotational motions of the nanogenerator. (f) Voltage response curves with sunlight irradiation time. (g) The variation of electrical signal period with the intensity of sunlight. Reproduced from ref. 102 with permission from American Chemical Society, copyright 2022.

weight of a wooden block, moving 18.5 cm every 36 s and rotating 153° every 23 s. The photothermal actuator has recently been used for rotational motion, which is utilized to rotate the rotor of an electric nanogenerator for determining sunlight's intensity and generating electrical energy.[102,205] As shown in Fig. 10e, the triboelectric nanogenerator is fabricated by black silicon and copper foam. The self-propulsion converts light into an electrical signal, generating an open circuit voltage of 2.35 V (Fig. 10f and g).

5.3. Jumping robots

Jumping motion is preferred over crawling motion in artificial robotic systems due to its higher efficiency and faster locomotion. Certain insect larvae can jump by compressing their bodies and releasing stored elastic energy, while insect–parasitic nematodes jump towards their hosts using surface tension and volatile cues.[206,207] Xu *et al.* have designed a soft jumping actuator using a MXene/PDMS bilayer composite film inspired by gall midge larvae.[208] The movement is mainly due to the light-induced deformation of the MXene composite film, the elasticity of the loop structure, and the storage and release of elastic deformation energy caused by the latch. Lei and colleagues developed a jumping soft actuator that imitates the motion of *Asphondylia*.[209] The actuator is formed by connecting the ends of an LCE polymer film using a light lock, which results in a closed-loop structure that stores elastic energy (Fig. 11a–c). The actuator exhibits outstanding performance, with a maximum jumping height of 10 body lengths and a take-off velocity of 62 body lengths per second when exposed to 460 nm LED irradiation. The iron oxide nanoparticle embedded poly(sodium acrylate) in-air hydrogel showed a fast response jumping and rolling hydrogel actuator driven by NIR light.[210] The hydrogel actuator's temperature quickly rises due to the photothermal effect, causing water to vaporize and form a gas bubble. The expanding bubble hits the substrate, creating a force that makes it jump/roll. The precise control of the jumping motion for microrobots in dynamic and cluttered environments is a significant challenge, especially when delivering payloads to targeted locations due to surface properties and irregularities.

5.4. Motors

The rolling motion of a motor on a flat surface is more significant than its crawling and jumping motion. When non-uniform illumination (NIR) is applied to the photothermal actuator motor, the curvature on the light-facing side diminishes, which generates a torque that propels the motor away from the light source. Cheng *et al.* created photothermal-actuated rolling robots.[212] The process involved cutting a monodomain film into strips, which were then rolled into tubes and reinforced with plastic rings to create a rolling soft robot. The robot was capable of navigating through various routes using

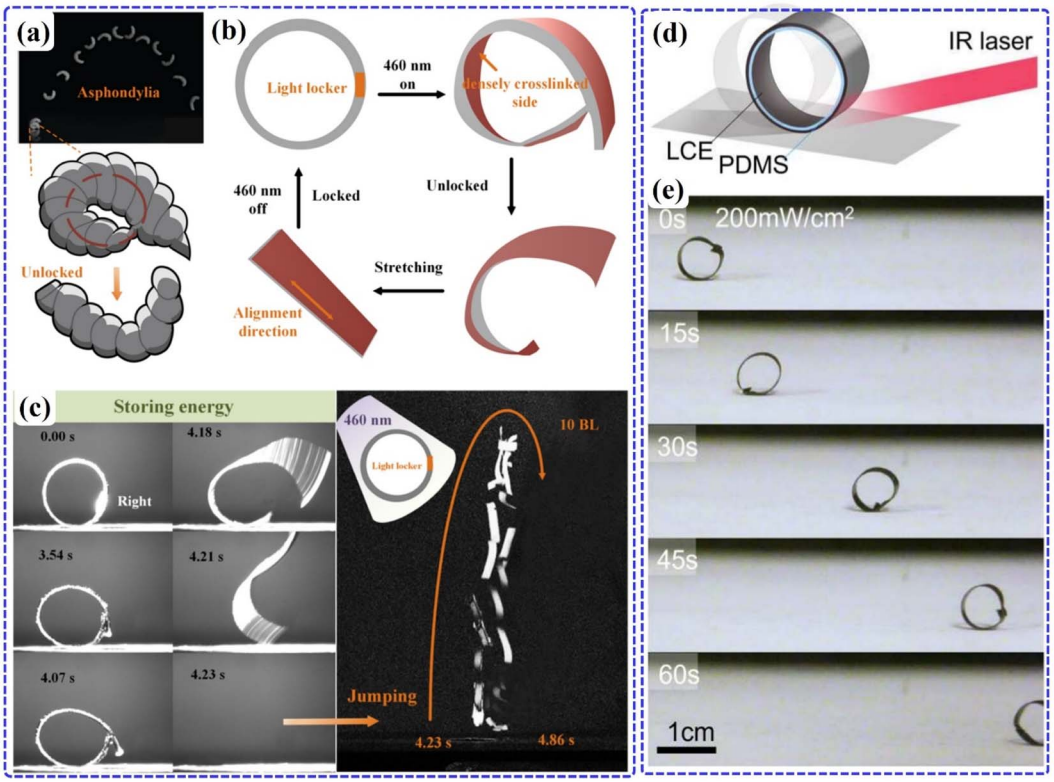

Fig. 11 (a) Images of the jumping *Asphondylia* and (b) schematic diagram of the locking and unlocking process of the soft actuator by a 460 nm light stimulus. (c) The jumping process of the LCE soft actuator. Reproduced from ref. 209 with permission from American Chemical Society, copyright 2023. (d and e) Schematic and sequential snapshots of a roller. Reproduced from ref. 211 with permission from Science, copyright 2023.

light guidance and could climb a slope of 6° within 20 s. Wang *et al.* have developed a rolling motor using a stacked graphene assembly/polyethylene (SGA/PE) bilayer film actuator.[15] Its motion is initiated by heating the outer layer with IR light, causing it to interact with the ground and move forward. This bilayer can also climb obstacles and move on wavy sandy ground. The SGA/PE rolls also enable the assembly of a bi-wheel and four-wheel chassis system. Zhao and colleagues developed a soft robotic actuator using a CS doped LCE/PDMS bilayer film.[211] This actuator achieved a rolling motion at a speed of 72 mm min^{-1} when exposed to NIR light at an intensity of 200 mW cm^{-2}. The rolling was produced by illuminating only one side of the roller, causing curvature change on the illuminated side, which in turn altered the roller's center of mass and enabled it to roll on the surface (Fig. 11d and e). This development represents a significant step forward in the creation of small, versatile rolling robots in the future.

5.5. Mechanical grippers

Photothermal grippers are advanced devices that enable non-contact manipulation, adaptive gripping, and serve as an artificial muscle for biomimetic applications across various robotic systems. Zhang *et al.* have created bionic devices such as simulated gestures, a soft gripper, a bionic flower, and a light-controlled smart switch using a $Ti_3C_2T_x$-delignified wood/low-density polyethylene bilayer actuator.[213] The gripper is made up of four rectangular actuators that generate thermal deformation to move closer and grab a polyfoam desk. Xue *et al.* have recently developed new conductive hydrogel based soft actuators by using conductive surface functionalized MXene/poly(3,4-ethylenedioxythiophene)/poly(styrenesulfonate) (K-MXene/PEDOT:PSS) ink and PNIPAM hydrogels.[214] The soft gripper can detect gripping and non-gripping actions, making it useful for soft robotics and intelligent machines. The tendrils of climbing plants exhibit helical growth in response to sunlight. When the tip-sensitive region encounters an obstacle, it triggers an electrophysiological response causing the tendrils to bend towards the obstacle. This mechanism has potential for creating a programmable photothermal actuator. Li *et al.* developed liquid metal/polyimide/polytetrafluoroethylene (LM/PI/PTFE) programmable photothermal actuators inspired by climbing plant tendrils.[215] The grasping robot, as depicted in Fig. 12a, was designed to mimic an eagle's claw. When the NIR laser irradiates the claw, it opens; similarly, when simulated sunlight is applied, the arm opens the helix, and the claw moves downward. By employing two light sources in conjunction, the grasping robot is capable of remotely grasping and releasing a ball. These advancements in soft robotics have immense potential to revolutionize the field and create new opportunities for intelligent robots.

5.6. Smart switches

In contrast to a simple on/off switch, the photothermal actuator-based switch exhibits exceptional performance for advanced electronic technology due to the rapid light response and speed of the actuator. The photothermal switch can switch on or off a circuit at a specific intensity of light. Bai *et al.* created shape memory ionomers by cross-linking PVA and polyacrylic acid with metal ions for switches.[100] They designed light-operated switches based on these materials that can turn lamps on or off with NIR light. Liu *et al.* have utilized photothermal actuators to control the on–off state of an LED using an external light source.[216] The actuator is connected to the circuit which switches on an LED light during the night. During the day or when exposed to light, the actuators bend and disconnect the circuit, resulting in the LED being in the off state. Once the external light source is removed, the actuator gradually returns to connect the circuit, and the LED is turned on again. This smart light-driven switch mechanism is illustrated in Fig. 12b and c. A recent study by Liu *et al.* has introduced a new type of photothermal actuator based on a MXene material that can generate phototropic deformation and self-sustained

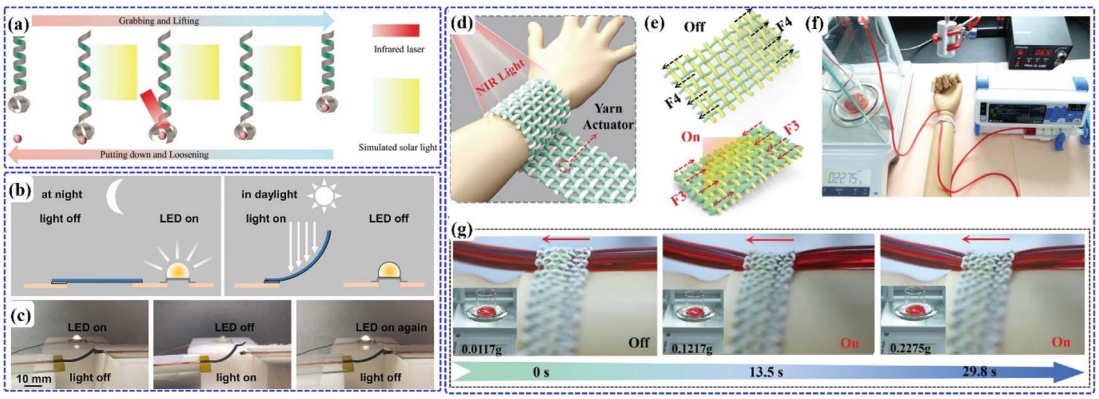

Fig. 12 (a) Mechanism of an LM/PI/PTFE grasping robot. Reproduced from ref. 215 with permission from Wiley-VCH GmbH, copyright 2024. (b) Schematic illustration and (c) optical image of the working process of photothermal actuator switches. Reproduced from ref. 216 with permission from American Chemical Society, copyright 2023. (d and e) Schematic illustration and actuation mechanism of hemostatic bandage, under light illumination, respectively. (f) Optical image showing a light-controlled hemostatic bandage regulating fluid flow on a synthetic arm. (g) Optical image of the tightening infusion tube by hemostatic bandage under light. Reproduced from ref. 217 with permission from Wiley-VCH GmbH, copyright 2024.

Table 3 Advantages and limitations of photothermal actuators based on their actuation mechanism, design and performance

Photothermal actuation mechanism	Materials	Light source/ intensity	Photothermal conversion mechanism	Response time	Motion performance	Application	Advantages	Limitations	Ref.
Surface tension gradient	CuS/PNIPAM	NIR laser/2 W cm^{-2}	NRR	5.5 s	Linear speed: 4.3 cm s^{-1}	Swimming robot	• Flexibility in material selection	• Work on air/liquid or liquid/liquid interface	158
	PDA–HGMPs/ PNIPAM	NIR laser/7 W cm^{-2}	TVM	—	Floating speed: 17 mm s^{-1} Sinking speed: 14.6 mm s^{-1}	Swimming robot	• Produces heat induced surface tension gradient	• Non-wettable surface is crucial	163
	Mg–MG/PHA	NIR laser/2 W cm^{-2}	PLH	3 s	Linear speed: 9.91 mm s^{-1}	Swimming robot	• Environment friendly actuation	• High-intensity light source is crucial	221
	PVDF/$Ti_3C_2T_x$	NIR laser/2 W cm^{-2}	NRR	—	Vertical speed: 7.3 mm s^{-1} Horizontal speed: 6 mm s^{-1}	Non-aqueous liquid robot			161
	Oxazine hydrogel	Visible light/ 19 W cm^{-2}	TVM	—	Linear speed: 14.53 mm s^{-1}	Swimming robot			159
	Candle soot/ PDMS	IR laser, sunlight/2 W cm^{-2}	TVM	—	Linear speed: 0.19 m s^{-1} Rotational speed: 43.2 rad s^{-1}	Swimming actuator			162
	MWCNT/PDMS	NIR laser/20 W cm^{-2}	TVM	0.2 s	Linear speed: 4.19 cm s^{-1} Angular speed: 5.3 rad s^{-1}	Swimming robot			157
	LIG tape	Blue laser	TVM	1 s	Linear speed: 2.9 mm s^{-1} Rotational speed: 3.8° s^{-1}	Swimming robot			95
	A-CNT/carbon foam	NIR laser/2.5 W cm^{-2}	TVM	0.3 s	Linear speed: 1.92 cm s^{-1} Rotational speed: 0.45–0.39 rad s^{-1}	Swimming robots			222
Expansion/ contraction	Liquid metal/ polyimide	NIR laser/1.5 W cm^{-2}	PLH	—	Bending speed: 21.89° s^{-1} Swimming speed: 0.91 mm s^{-1}	Crawling, swimming robot	• Fast actuation • High bending	• Dissimilar thermal expansive materials required for layer actuator	223
	K-MXene/ PEDOT:PSS/ PNIPAM hydrogels	NIR laser/1.2 W cm^{-2}	NRR	3 s	—	Gripper	• Flexibility in material selection		214
	PNIPAM/P-MXene/Ca^{2+} hydrogel	NIR laser/0.4 W cm^{-2}	NRR	10 s	—	Gripper	• Excellent mechanical stability		168
	Carbon black layer/PET film/ acrylic adhesive	NIR laser/150 mW cm^{-2}	TVM	0.36 s	Bending speed: 72.5° s^{-1} Light mill rotation speed: 19 rpm Crawling speed: 26 mm s^{-1}	Crawler, light mill, gripper			170
	LM/PI/PTFE	NIR laser/ 1.25 W cm^{-2}	PLH	—	Swimming speed: 3.07 mm s^{-1} Rotational speed: 20.77° s^{-1}	Gripper, crawling robot, rotor			215
	GO/PDMS	NIR laser/800 mW cm^{-2}	TVM	400 ms	Jumping speed: 2 m s^{-1}	Jumping robot			5
	Polycaprolactone diol–PDA	Green light/ 300 mW cm^{-2}	TVM	—	—	Switches			224

Table 3 (*Contd.*)

Photothermal actuation mechanism	Materials	Light source/ intensity	Photothermal conversion mechanism	Response time	Motion performance	Application	Advantages	Limitations	Ref.
	PU/modified graphene	NIR laser/0.8 W cm^{-2}	TVM	1 s	Linear speed: 2.67 BL per s	Swimming robot			99
	CNT/paraffin wax/Kapton film	Visible light/ 100 mW cm^{-2}	TVM	1 s	Bending speed: 54.5–97.7° s^{-1}	Mechanical arm			80
	MiniGNR nanomonomer/ LCN	NIR laser/300 mW cm^{-2}	PLH	2.3 s	Bending speed: 50.4° s^{-1} Crawling speed: 5.7 mm s^{-1}	Crawling robot			202
Phase transition	PNIPAM-*g*-MC/ magnetite nanoparticle	Visible light/ 41.3 mW cm^{-2}	NRR	30 s	Linear swelling ratio: 3.43 to 1.57	Static-motion actuators	• Rapid change in shape or volume	• Requirement of special material	225
	Graphene/PDMS	NIR laser	TVM	—	—	Gripper, sensor, crawling robot	• Fast response times	• Higher temperature sensitive	103
	Dichroic/LCEs	Laser/150 mW cm^{-2}	TVM	0.11 s	Rotational speed: 30 rpm	Light mill	• Large-scale deformations		226
	Au/LCE Ag/LCE	Visible light	PLH	—	—	Switches	• Flexibility and versatility in design and performance		227
	Au/silicone elastomers	NIR laser/475 mW cm^{-2}	PLH	—	—	Soft valve, crawling robot			228
	MXene–LCE	NIR laser/500 mW cm^{-2}	NRR	18 s	Bending speed: 5° s^{-1}	Light-tracking robot			229
	Polyolefin elastomer/ paraffin wax/ CNTs	IR light/200 mW cm^{-2}	TVM	—	—	Gripper, bionic walking robot, temperature sensor			230
	2D-Cu nanosheet/LCE	NIR laser/1 W cm^{-2}	PLH	8 s	Crawling speed: 4 cm min^{-1} Windmill speed: 3 rpm	Gripper, windmill, crawling robot			231
	CNT/LCE	IR light/ 149.74 W m^{-2}	TVM	3 s	Shrinkage: 70%	Artificial muscle actuators			220
	AuNRs/LCE	NIR laser/600 mW cm^{-2}	PLH	—	Swimming speed: 1.9 mm s^{-1}	Swimming robot, wearing actuator			217

oscillation with tunable frequency and amplitude under constant light in air.[218] This actuator can be used as a switch to control the signal lamp's three states, including lamp off, light on, and flashing, by only adjusting the light intensity.

5.7. Wearable cloths

Breathable fabrics are important for wearable applications during exercise. Embedding photo-thermal responsive actuators in clothing can create a breathable device that operates based on light or body temperature.[219] Zhao *et al.* have developed a smart breathable fabric inspired by the stomata of plant leaves.[69] The fabric uses photothermal bimorph textile actuator-based yarns that bend when the temperature rises under simulated sunlight, allowing more air flow between the skin and the outside. In nature, spiders produce silk that exhibits rapid contraction and deformation in response to environmental stimuli. This unique property has served as inspiration for the development of yarn actuators used in soft robot energy transmission. LCE fibers have a high degree of shape variability and excellent wear resistance when subjected to external stimuli, rendering them well-suited for applications in smart textiles and soft robotics.[220] Wu *et al.* have developed an AuNRs@LCE active yarn that exhibits significant contraction and stable actuation characteristics.[217] A liquid crystal oligomer solution was electrospun to form micro/nanofibers, which were then twisted, cross-linked using UV, and subjected to a drafting. The active yarn demonstrated long-term stability in light absorption and actuation capabilities. Leveraging its flexibility, the authors have developed light-controlled super-contractile smart hemostatic bandages (Fig. 12d and e). Cotton serves as the weft yarn in the bandage and the actuator serves as the warp yarn. By heating and contracting the active yarn with NIR light, the infusion tube on the arm is tightened, lowering the flow rate (Fig. 12f and g). This development paves the way for the production of smart wearables and soft actuators utilizing the generated LCE active yarn.

6. Conclusions, challenges and future perspectives

In this review, we explore the core concepts of the photothermal effect and photothermal actuation mechanisms, the latest developments in photothermal soft actuators, and emerging applications. The straightforward design concept, which involves integrating a photothermal active layer with a passive layer in a single actuating system, is highly favored by researchers for designing photothermal actuators. These actuators have outstanding features such as programmability, reconfigurability, ultra-sensitivity, versatility, and exceptional actuating performance.

Photothermal actuators utilize photothermal materials such as metallic nanoparticles, semiconducting nanomaterials, and organic photothermal materials. These materials have broad light absorption and exceptional photothermal conversion capabilities. They can be controlled using light with adjustable physical characteristics like intensity, wavelength, and polarization, making them ideal for photothermal soft actuators. By using light as stimuli, the thermal gradients, position, and motion of photothermal actuators can be controlled remotely. These actuators are operated by visible light, NIR, UV, and sunlight. The light-induced heat leads to movement on liquid surfaces or shape changes in polymers. These actuators have fast response and outstanding performance in various applications including soft crawling robot, jumping robot, switches, motors, aquatic robots, soft grippers and wearable actuators. The potential for synergy is found in combining superhydrophobic properties with photothermal actuators to enable intelligent movement in underwater environments. Various structured photothermal actuators have been designed to meet the demands of different applications. These include bilayer, multilayer, hydrogel, gradient structure, composite membrane, film, strip, micro-gear, foam, and nanofiber actuators. All these actuators show exceptional photothermal actuation performance. However, the use of photothermal nanomaterials in photothermal actuators presents challenges and limitations. Incorporating these materials into the polymer matrix can lead to aggregation and reduced optical transparency, which ultimately diminishes conversion efficiency and impacts actuator performance. Additionally, excessive use of organic or inorganic materials can result in environmental issues. Table 3 summarizes the advantages and challenges of photothermal actuators based on their actuation mechanism and performance. Photothermal soft actuators have the potential to enable the development of bioinspired soft robotics with programmable and reconfigurable functions, thus expanding the range of robotic applications.

Nevertheless, several obstacles prevent light-driven photothermal actuators from being widely used, and these are outlined below,

(1) The polymer used as a substrate and adhesive has low thermal conductivity, resulting in slow heating and cooling. High temperatures during the photothermal conversion process can cause interfacial failure and poor surface stability. To overcome this, high-temperature resistant materials that heat and cool rapidly need to be developed.

(2) The actuator must be multifunctional to suit different applications. It should have features like obstacle avoidance for micro-robots, flexibility and oil-collection for water-cleaning. Additionally, it must have improved light response and moving velocity to enable high-speed light-driven operation.

(3) Actuator preparation using photothermal materials is complex, and the superhydrophobic modification process involves harmful fluorine-containing reagents. To enable widespread implementation of the technology, it is essential to fabricate actuators from environmentally friendly, superhydrophobic photothermal materials.

(4) A lot of recent studies on these actuators do not delve into the study of the physical mechanisms that drive their operation. Thus, a more in-depth comprehension of the actuator motion from the perspective of fluid dynamics and light-to-heat conversion could further broaden the range of applications for these actuators in the mechanical engineering field.

(5) Photothermal actuators have potential for use in soft robots, grippers, and bionic movements. However, their application for bird-like flying is limited due to lower response speed and small deforming forces. Soft photothermal actuators can be researched for potential use in space missions, planetary rovers, and manipulators for tasks like sample collection and exploration.

(6) Photothermal soft actuators are ideal for aerospace and defense applications, particularly for tasks such as adaptive structures, morphing wings, and unmanned aerial vehicles (UAVs). Their lightweight and conformable properties make them well-suited for applications requiring agility, stealth, and resilience.

Data availability

No primary research results, software or code have been included and no new data were generated or analysed as part of this review.

Author contributions

Rajaram S. Sutar: conceptualization, investigation, writing – original draft; Sanjay S. Latthe: investigation, validation, writing – review & editing; Xinna Wu: investigation, data curation; Kazuya Nakata: investigation, validation; Ruimin Xing: investigation, writing – review & editing, supervision, validation; Shanhu Liu: conceptualization, investigation, writing – review & editing, project administration, supervision; Akira Fujishima: investigation, validation.

Conflicts of interest

There are no conflicts to declare.

Acknowledgements

We greatly appreciate the support of the National Natural Science Foundation of China (21950410531), Science and Technology Research Project of Henan Province (242102240045), and the Petro-China Research Institute of Petroleum Exploration & Development (RIPED-2019-CL-186). One of the authors, SSL, is grateful for financial assistance received through the Seed Money Scheme from Vivekanand College, Kolhapur (Empowered Autonomous), Ref. No. VCK/3108/2023-24 dated 30/03/2024.

References

1 J. Lee, Y. Yoon, H. Park, J. Choi, Y. Jung, S. H. Ko and W.-H. Yeo, *Adv. Intell. Syst.*, 2022, **4**, 2100271.
2 L. Wang, M. Zhao, Y. He, S. Ding and L. Sun, *Soft Matter*, 2023, **19**, 2883–2890.
3 Z. Bi, Q. Zhou and H. Fang, *Int. J. Mech. Sci.*, 2023, **254**, 108436.
4 D. Shen, Q. Zhang, C. Wang, X. Wang and M. Tian, *IEEE Rob. Autom. Lett.*, 2021, **6**, 3744–3751.
5 Y. Xiang, B. Li, B. Li, L. Bao, W. Sheng, Y. Ma, S. Ma, B. Yu and F. Zhou, *ACS Appl. Mater. Interfaces*, 2022, **14**, 20291–20302.
6 S. Wu, Y. Hong, Y. Zhao, J. Yin and Y. Zhu, *Sci. Adv.*, 2023, **9**, eadf8014.
7 R. Bernasconi, D. Carniani, M.-S. Kim, S. Pané and L. Magagnin, *ACS Appl. Mater. Interfaces*, 2022, **15**, 2396–2408.
8 H. Zhu, B. Xu, Y. Wang, X. Pan, Z. Qu and Y. Mei, *Sci. Robot.*, 2021, **6**, eabe7925.
9 Y. Cheng, K. Ren, D. Yang and J. Wei, *Sens. Actuators, B*, 2018, **255**, 3117–3126.
10 L. Sun, L. Che, M. Li, W. G. Neal, X. Leng, Y. Long, Y. Jia, Y. Gao, M. Palma and Y. Lu, *SusMat*, 2023, **3**, 207–221.
11 J. Xue, Y. Ge, Z. Liu, Z. Liu, J. Jiang and G. Li, *ACS Appl. Mater. Interfaces*, 2022, **14**, 10836–10843.
12 X.-J. Luo, L. Li, H.-B. Zhang, S. Zhao, Y. Zhang, W. Chen and Z.-Z. Yu, *ACS Appl. Mater. Interfaces*, 2021, **13**, 45833–45842.
13 J. Zhao, Q. Li, B. Miao, H. Pi and P. Yang, *Small*, 2020, **16**, 2000043.
14 H. Chathuranga, I. Marriam, S. Chen, Z. Zhang, J. MacLeod, Y. Liu, H. Yang and C. Yan, *ACS Appl. Mater. Interfaces*, 2022, **14**, 16772–16779.
15 S. Wang, Y. Gao, A. Wei, P. Xiao, Y. Liang, W. Lu, C. Chen, C. Zhang, G. Yang and H. Yao, *Nat. Commun.*, 2020, **11**, 4359.
16 Y. Ling, W. Pang, J. Liu, M. Page, Y. Xu, G. Zhao, D. Stalla, J. Xie, Y. Zhang and Z. Yan, *Nat. Commun.*, 2022, **13**, 524.
17 H. Wang, Z. Zhao, P. Liu, Y. Pan and X. Guo, *ACS Appl. Mater. Interfaces*, 2022, **14**, 41283–41295.
18 X. Wang, D. Lin, Y. Zhou, N. Jiao, S. Tung and L. Liu, *ACS Nano*, 2022, **16**, 14895–14906.
19 F. Xiong, L. Zhang, L. Xu, H. Zhao, J. Lan, C. Ji, L. Chen and F. Xia, *NPG Asia Mater.*, 2022, **14**, 84.
20 Z. Li, P. Liu, X. Ji, J. Gong, Y. Hu, W. Wu, X. Wang, H. Q. Peng, R. T. Kwok and J. W. Lam, *Adv. Mater.*, 2020, **32**, 1906493.
21 L. Yang, J. Cui, L. Zhang, X. Xu, X. Chen and D. Sun, *Adv. Funct. Mater.*, 2021, **31**, 2101378.
22 W. Zeng, C. Jiang and D. Wu, *ACS Appl. Mater. Interfaces*, 2023, **15**, 16097–16108.
23 M. Zhang, H. Shen, K. Hakobyan, Z. Jiang, K. Liang and J. Xu, *Small*, 2024, 2400534.
24 Z. Zhang and W. Yuan, *Compos. Sci. Technol.*, 2023, **242**, 110185.
25 D. Li, J. Zhou, Z. Zhao, X. Huang, H. Li, Q. a. Qu, C. Zhou, K. Yao, Y. Liu and M. Wu, *Sci. Adv.*, 2024, **10**, eadk6301.
26 C. Liu, H. Xu, Y. Liang, S. Ma, Z. Lin, L. Ren, Z. Han and L. Ren, *Chem. Eng. J.*, 2023, **472**, 144700.
27 X. Liu, L. Wang, Y. Xiang, F. Liao, N. Li, J. Li, J. Wang, Q. Wu, C. Zhou and Y. Yang, *Sci. Robot.*, 2024, **9**, eadh2479.
28 R. Xie, Y. Cao, R. Sun, R. Wang, A. Morgan, J. Kim, S. J. Callens, K. Xie, J. Zou and J. Lin, *Sci. Adv.*, 2024, **10**, eadl1549.
29 C. Shen, R. Lan, R. Huang, Z. Zhang, J. Bao, L. Zhang and H. Yang, *ACS Appl. Mater. Interfaces*, 2021, **13**, 3221–3227.

30 W. Xu, D. M. Sanchez, U. Raucci, H. Zhou, X. Dong, M. Hu, C. J. Bardeen, T. J. Martinez and R. C. Hayward, *Nat. Mater.*, 2023, 1–8.
31 H. Li, Z. Wu, Y. Xing, B. Li and L. Liu, *Nano Energy*, 2022, **103**, 107821.
32 D. Wu, Y. Zhang, H. Yang, A. Wei, Y. Zhang, A. Mensah, R. Yin, P. Lv, Q. Feng and Q. Wei, *Mater. Horiz.*, 2023, **10**, 2587–2598.
33 J. W. Mao, D. D. Han, H. Zhou, H. B. Sun and Y. L. Zhang, *Adv. Funct. Mater.*, 2023, **33**, 2208677.
34 J. Wang, P. Li, Z. Jing, T. Leydecker, A. Neogi and Z. Wang, *Adv. Opt. Mater.*, 2023, **11**, 2202201.
35 S. Iamsaard, E. Anger, S. J. Aßhoff, A. Depauw, S. P. Fletcher and N. Katsonis, *Angew. Chem.*, 2016, **128**, 10062–10066.
36 A. S. Kuenstler, K. D. Clark, J. R. de Alaniz and R. C. Hayward, *ACS Macro Lett.*, 2020, **9**, 902–909.
37 M. Lahikainen, H. Zeng and A. Priimagi, *Nat. Commun.*, 2018, **9**, 4148.
38 X. Lu, H. Zhang, G. Fei, B. Yu, X. Tong, H. Xia and Y. Zhao, *Adv. Mater.*, 2018, **30**, 1706597.
39 M. R. Molla, P. Rangadurai, L. Antony, S. Swaminathan, J. J. de Pablo and S. Thayumanavan, *Nat. Chem.*, 2018, **10**, 659–666.
40 D. Kim, H. S. Lee and J. Yoon, *Sci. Rep.*, 2016, **6**, 20921.
41 A. S. Kuenstler and R. C. Hayward, *Curr. Opin. Colloid Interface Sci.*, 2019, **40**, 70–86.
42 C. Li, A. Iscen, L. C. Palmer, G. C. Schatz and S. I. Stupp, *J. Am. Chem. Soc.*, 2020, **142**, 8447–8453.
43 T. Wang, J. Huang, Y. Yang, E. Zhang, W. Sun and Z. Tong, *ACS Appl. Mater. Interfaces*, 2015, **7**, 23423–23430.
44 J. Gao, Y. Tang, D. Martella, J. Guo, D. S. Wiersma and Q. Li, *Responsive Materials*, 2023, **1**, e20230008.
45 Y.-L. Guo, J. Zhou, Y. Huang and M. H. Bao, *Sensors*, 2007, **7**, 1713–1719.
46 T. Zhang, H. Chang, Y. Wu, P. Xiao, N. Yi, Y. Lu, Y. Ma, Y. Huang, K. Zhao and X.-Q. Yan, *Nat. Photonics*, 2015, **9**, 471–476.
47 G. Eda, C. Mattevi, H. Yamaguchi, H. Kim and M. Chhowalla, *J. Phys. Chem. C*, 2009, **113**, 15768–15771.
48 J. Kim, J. Oh, C. In, Y.-S. Lee, T. B. Norris, S. C. Jun and H. Choi, *ACS Nano*, 2014, **8**, 2486–2494.
49 B. F. Lui and C. J. Bardeen, *Small*, 2022, **18**, 2105356.
50 X. Cui, Q. Ruan, X. Zhuo, X. Xia, J. Hu, R. Fu, Y. Li, J. Wang and H. Xu, *Chem. Rev.*, 2023, **123**, 6891–6952.
51 S. Watanabe, K. Arikawa, M. Uda, S. Fujii and M. Kunitake, *Langmuir*, 2021, **37**, 14597–14604.
52 J. Chen, Y. Cao, J. Pei and H. Zhao, *ACS Appl. Mater. Interfaces*, 2023, **5**, 31917–31926.
53 X. Zhang, Z. Yu, C. Wang, D. Zarrouk, J.-W. T. Seo, J. C. Cheng, A. D. Buchan, K. Takei, Y. Zhao and J. W. Ager, *Nat. Commun.*, 2014, **5**, 2983.
54 G. Cai, J.-H. Ciou, Y. Liu, Y. Jiang and P. S. Lee, *Sci. Adv.*, 2019, **5**, eaaw7956.
55 Z. Wan, C. Li, R. Liu, W. Zhou, W. Fan, C. Huang and Y. Liu, *ACS Appl. Mater. Interfaces*, 2024, **16**, 4999–5008.
56 Z. Chen, R. Cao, S. Ye, Y. Ge, Y. Tu and X. Yang, *Sens. Actuators, B*, 2018, **255**, 2971–2978.
57 Q. Guo, C. Li, K. Yang, P. Zhou, N. Hua and M. Weng, *ACS Appl. Nano Mater.*, 2023, **6**, 4925–4935.
58 P. Zhou, L. Chen, L. Yao, M. Weng and W. Zhang, *Nanoscale*, 2018, **10**, 8422–8427.
59 X. Yu, H. Cheng, M. Zhang, Y. Zhao, L. Qu and G. Shi, *Nat. Rev. Mater.*, 2017, **2**, 1–13.
60 H. Zhou, H. Niu, H. Wang and T. Lin, *Chem. Rev.*, 2022, **123**, 663–700.
61 S. Li, Z. Cai, J. Han, Y. Ma, Z. Tong, M. Wang, L. Xiao, S. Jia and X. Chen, *RSC Adv.*, 2023, **13**, 18090–18098.
62 D. Niu, W. Jiang, H. Liu, T. Zhao, B. Lei, Y. Li, L. Yin, Y. Shi, B. Chen and B. Lu, *Sci. Rep.*, 2016, **6**, 27366.
63 G. Zhang, L. Yan, L. Ji, C. Liu, L. Zhang, W. Zhang, Y. Nie, P. Xiao and T. Chen, *Macromol. Mater. Eng.*, 2021, **306**, 2000502.
64 Y. Zhang, R. Wang, W. Tan, L. Yang, X. Lv, X. Wang, F. Wang and C. Zhang, *J. Mater. Chem. A*, 2023, **11**, 15670–15680.
65 L. Kaushik, P. Raturi and J. Singh, *Sci. Rep.*, 2018, **8**, 3687.
66 D. Gao, M.-F. Lin, J. Xiong, S. Li, S. N. Lou, Y. Liu, J.-H. Ciou, X. Zhou and P. S. Lee, *Nanoscale Horiz.*, 2020, **5**, 730–738.
67 B. Li, Y. Zhang, T. Li, H. Yu, Q. Guo, M. Hu and J. Yang, *Macromol. Mater. Eng.*, 2022, **307**, 2100868.
68 Q. Li and Y. Jiao, *ACS Appl. Mater. Interfaces*, 2022, **14**, 55828–55838.
69 H. Zhao, X. Qi, Y. Ma, X. Sun, X. Liu, X. Zhang, M. Tian and L. Qu, *Nano Lett.*, 2021, **21**, 8126–8134.
70 J. Chen, S. Sun, M. M. Macios, E. Oguntade, A. R. Narkar, P. T. Mather and J. H. Henderson, *ACS Appl. Mater. Interfaces*, 2023, **15**, 50962–50972.
71 K. Wang and X. Zhu, *ACS Biomater. Sci. Eng.*, 2018, **4**, 3099–3106.
72 F. Zhao, W. Rong, L. Wang and L. Sun, *ACS Appl. Mater. Interfaces*, 2023, **15**, 25942–25951.
73 C. P. Ambulo, M. J. Ford, K. Searles, C. Majidi and T. H. Ware, *ACS Appl. Mater. Interfaces*, 2020, **13**, 12805–12813.
74 A. Potekhina and C. Wang, *Adv. Mater. Technol.*, 2022, **7**, 2101732.
75 N. P. Skillin, G. E. Bauman, B. E. Kirkpatrick, J. M. McCracken, K. Park, R. A. Vaia, K. S. Anseth and T. J. White, *Adv. Mater.*, 2024, 2313745.
76 Y.-Y. Xiao, Z.-C. Jiang, J.-B. Hou and Y. Zhao, *Nat. Commun.*, 2021, **12**, 624.
77 C. Zhu, Y. Lu, L. Jiang and Y. Yu, *Adv. Funct. Mater.*, 2021, **31**, 2009835.
78 T. Wang, J. Zhao, C. Weng, T. Wang, Y. Liu, Z. Han and Z. Zhang, *Composites, Part A*, 2021, **144**, 106322.
79 X. Zhang, M. Jin, L. Ding, J. He, Y. Bai and L. Zhang, *Chem. Eng. J.*, 2023, **468**, 143734.
80 J. Deng, J. Li, P. Chen, X. Fang, X. Sun, Y. Jiang, W. Weng, B. Wang and H. Peng, *J. Am. Chem. Soc.*, 2016, **138**, 225–230.
81 Y. Hu, G. Wu, T. Lan, J. Zhao, Y. Liu and W. Chen, *Adv. Mater.*, 2015, **27**, 7867–7873.
82 E. Lee, D. Kim, H. Kim and J. Yoon, *Sci. Rep.*, 2015, **5**, 15124.
83 H. Ma, J. Hou, X. Wang, J. Zhang, Z. Yuan, L. Xiao, Y. Wei, S. Fan, K. Jiang and K. Liu, *Nano Lett.*, 2017, **17**, 421–428.

84 T. Wang, D. Torres, F. E. Fernández, A. J. Green, C. Wang and N. Sepúlveda, *ACS Nano*, 2015, **9**, 4371–4378.
85 B. Han, Y. L. Zhang, L. Zhu, Y. Li, Z. C. Ma, Y. Q. Liu, X. L. Zhang, X. W. Cao, Q. D. Chen and C. W. Qiu, *Adv. Mater.*, 2019, **31**, 1806386.
86 M. Ji, N. Jiang, J. Chang and J. Sun, *Adv. Funct. Mater.*, 2014, **24**, 5412–5419.
87 J. Li, Y. Tao, S. Chen, H. Li, P. Chen, M.-z. Wei, H. Wang, K. Li, M. Mazzeo and Y. Duan, *Sci. Rep.*, 2017, **7**, 16468.
88 M. Weng, P. Zhou, L. Chen, L. Zhang, W. Zhang, Z. Huang, C. Liu and S. Fan, *Adv. Funct. Mater.*, 2016, **26**, 7244–7253.
89 Y. Zhang, J. B. Chou, J. Li, H. Li, Q. Du, A. Yadav, S. Zhou, M. Y. Shalaginov, Z. Fang and H. Zhong, *Nat. Commun.*, 2019, **10**, 4279.
90 H. Arazoe, D. Miyajima, K. Akaike, F. Araoka, E. Sato, T. Hikima, M. Kawamoto and T. Aida, *Nat. Mater.*, 2016, **15**, 1084–1089.
91 Z. Cheng, T. Wang, X. Li, Y. Zhang and H. Yu, *ACS Appl. Mater. Interfaces*, 2015, **7**, 27494–27501.
92 W. Wei, Z. Zhang, J. Wei, X. Li and J. Guo, *Adv. Opt. Mater.*, 2018, **6**, 1800131.
93 H. Yang, W. R. Leow, T. Wang, J. Wang, J. Yu, K. He, D. Qi, C. Wan and X. Chen, *Adv. Mater.*, 2017, **29**, 1701627.
94 T. Wang, D. Torres, F. E. Fernández, C. Wang and N. Sepúlveda, *Sci. Adv.*, 2017, **3**, e1602697.
95 W. Wang, B. Han, Y. Zhang, Q. Li, Y. L. Zhang, D. D. Han and H. B. Sun, *Adv. Funct. Mater.*, 2021, **31**, 2006179.
96 Y. Yamamoto, K. Kanao, T. Arie, S. Akita and K. Takei, *ACS Appl. Mater. Interfaces*, 2015, **7**, 11002–11006.
97 C. Yu, X. Li, X. Yang, X. Qiu, X. Zhang, Z. Chen and Y. Luo, *Small*, 2024, 2311656.
98 X.-w. Ning, T. Wu, Y. Du, H. Xie and J.-p. Qu, *Chem. Eng. J.*, 2023, **467**, 143555.
99 Y. Wang, G. Su, J. Li, Q. Guo, Y. Miao and X. Zhang, *Nano Lett.*, 2022, **22**, 5409–5419.
100 Y. Bai, J. Zhang, D. Wen, B. Yuan, P. Gong, J. Liu and X. Chen, *J. Mater. Chem. A*, 2019, **7**, 20723–20732.
101 K. X. Hou, P. C. Zhao and C. H. Li, *Adv. Opt. Mater.*, 2023, **11**, 2202949.
102 C. Liu, D. Jiang, G. Zhu, Z. Li, X. Zhang, P. Tian, D. Wang, E. Wang, H. Ouyang and M. Xiao, *ACS Appl. Mater. Interfaces*, 2022, **14**, 22206–22215.
103 Y. Shao, F. Long, Z. Zhao, M. Fang, H. Jing, J. Guo, X. Shi, A. Sun, G. Xu and Y. Cheng, *Chem. Eng. J.*, 2023, **454**, 140271.
104 S. M. Mirvakili and I. W. Hunter, *US Pat.*, No. 10935008, 2 Mar, 2021.
105 Y.-Y. Gao, B. Han, W.-Y. Zhao, Z.-C. Ma, Y.-S. Yu and H.-B. Sun, *Front. Chem.*, 2019, **7**, 506.
106 B. Han, Y. L. Zhang, Q. D. Chen and H. B. Sun, *Adv. Funct. Mater.*, 2018, **28**, 1802235.
107 Y. Huang, Q. Yu, C. Su, J. Jiang, N. Chen and H. Shao, *Actuators*, 2021, **10**, 298.
108 J. Li, X. Zhou and Z. Liu, *Adv. Opt. Mater.*, 2020, **8**, 2000886.
109 M. Yang, Z. Yuan, J. Liu, Z. Fang, L. Fang, D. Yu and Q. Li, *Adv. Opt. Mater.*, 2019, **7**, 1900069.
110 S. Cheng, S. S. Latthe, K. Nakata, R. Xing, S. Liu and A. Fujishima, *Mater. Today Chem.*, 2024, **35**, 101868.
111 M. Gao, L. Zhu, C. K. Peh and G. W. Ho, *Energy Environ. Sci.*, 2019, **12**, 841–864.
112 M. L. Brongersma, N. J. Halas and P. Nordlander, *Nat. Nanotechnol.*, 2015, **10**, 25–34.
113 J. G. Liu, H. Zhang, S. Link and P. Nordlander, *ACS Photonics*, 2017, **5**, 2584–2595.
114 W. Gärtner, *Phys. Rev.*, 1961, **122**, 419.
115 W. Shockley and W. Read Jr, *Phys. Rev.*, 1952, **87**, 835.
116 Y. Ye, J. He, H. Wang, W. Li, Q. Wang, C. Luo, X. Tang, X. Chen, X. Jin and K. Yao, *ACS Nano*, 2022, **16**, 18729–18745.
117 X. Yin, T. Fan, N. Zheng, J. Yang, L. Yan, S. He, F. Ai and J. Hu, *Nanoscale Adv.*, 2023, **5**, 1729–1739.
118 S. Yu, Q. Ke, F. Cai, S. Gong, R. Huang and C. Fan, *Sens. Diagn.*, 2023, **2**, 1605–1611.
119 J. Zhao, Y. Bai, Z. Li, J. Liu, W. Wang, P. Wang, B. Yang, R. Shi, G. I. Waterhouse and X. D. Wen, *Angew. Chem., Int. Ed.*, 2023, **62**, e202219299.
120 G. Zhou, Y. Chen, W. Chen, H. Wu, Y. Yu, C. Sun, B. Hu and Y. Liu, *Small*, 2023, **19**, 2206749.
121 H. Ge, Y. Kuwahara, M. Okada and H. Yamashita, *ACS Sustain. Chem. Eng.*, 2024, **12**, 2162–2171.
122 H. Li, K. Yang, L. Hai, Z. Wang, Y. Luo, L. He, W. Yi, J. Li, C. Xu and L. Deng, *Chem. Eng. J.*, 2023, **455**, 140903.
123 S. Mertens, B. Siegmund and K. Vandewal, *Mater. Horiz.*, 2023, **10**, 594–600.
124 K. Onishi, Y. Tokudome, K. Kariya, T. Kurokawa, H. Murata and A. Nakahira, *ACS Appl. Mater. Interfaces*, 2024, **16**, 16903–16911.
125 X.-H. Shi, L. Tao, L. Wang, X. Liu, S.-L. Liu and Z.-G. Wang, *Chem. Mater.*, 2024, **36**, 2776–2789.
126 P. Zhang, Y. Qiao, L. Zhu, M. Qin, Q. Li, C. Liu, Y. Xu, X. Zhang, Z. Gan and Y. Hou, *ACS Nano*, 2022, **17**, 184–196.
127 Y. Li, J. Wang, C. Fu, L. Huang, L. Chen, Y. Ni and Q. Zheng, *Energy Convers. Manage.*, 2023, **289**, 117160.
128 Z. Shi, M. Luo, Q. Huang, C. Ding, W. Wang, Y. Wu, J. Luo, C. Lin, T. Chen and X. Zeng, *Nat. Commun.*, 2023, **14**, 6567.
129 Y. Wang, W. Sha, M. Xiao, Y. Fang, Z. Wang, S. Wang, W. Zeng, J. Zhao and L. Ruan, *Chem. Eng. J.*, 2024, **489**, 151571.
130 S. K. Balu, R. Xing and S. Liu, *Sustainable Mater. Technol.*, 2024, e00941.
131 N. Bing, J. Yang, Y. Zhang, W. Yu, L. Wang and H. Xie, *Sustainable Energy Fuels*, 2020, **4**, 1208–1215.
132 Y. Hu, Q. Ji, M. Huang, L. Chang, C. Zhang, G. Wu, B. Zi, N. Bao, W. Chen and Y. Wu, *Angew. Chem.*, 2021, **133**, 20674–20680.
133 D. W. Kim, Y. Hagiwara, S. Hasebe, N. O. Dogan, M. Zhang, T. Asahi, H. Koshima and M. Sitti, *Adv. Funct. Mater.*, 2023, **33**, 2305916.
134 J. Zheng, X. Cheng, H. Zhang, X. Bai, R. Ai, L. Shao and J. Wang, *Chem. Rev.*, 2021, **121**, 13342–13453.
135 A. Agrawal, S. H. Cho, O. Zandi, S. Ghosh, R. W. Johns and D. J. Milliron, *Chem. Rev.*, 2018, **118**, 3121–3207.

136 J. Wang, Y. Li, L. Deng, N. Wei, Y. Weng, S. Dong, D. Qi, J. Qiu, X. Chen and T. Wu, *Adv. Mater.*, 2017, **29**, 1603730.
137 H. J. Kim, B. Kim, Y. Auh and E. Kim, *Adv. Mater.*, 2021, **33**, 2005940.
138 Z. Li, H. Lei, A. Kan, H. Xie and W. Yu, *Energy*, 2021, **216**, 119262.
139 Y. Ji, S. Moles Quintero, Y. Dai, J. M. Marín-Beloqui, H. Zhang, Q. Zhan, F. Sun, D. Wang, X. Li and Z. Wang, *Angew. Chem.*, 2023, **135**, e202311387.
140 F. Pujol-Vila, P. Güell-Grau, J. Nogués, M. Alvarez and B. Sepúlveda, *Adv. Funct. Mater.*, 2023, **33**, 2213109.
141 J. Zhang, H. Chen, X. Duan, H. Sun and S. Wang, *Mater. Today*, 2023, **68**, 234–253.
142 L. Scriven and C. Sternling, *Nature*, 1960, **187**, 186–188.
143 M. Gugliotti, M. S. Baptista and M. J. Politi, *J. Chem. Educ.*, 2004, **81**, 824.
144 W.-T. Cao, W. Feng, Y.-Y. Jiang, C. Ma, Z.-F. Zhou, M.-G. Ma, Y. Chen and F. Chen, *Mater. Horiz.*, 2019, **6**, 1057–1065.
145 W. Wang, Y. Q. Liu, Y. Liu, B. Han, H. Wang, D. D. Han, J. N. Wang, Y. L. Zhang and H. B. Sun, *Adv. Funct. Mater.*, 2017, **27**, 1702946.
146 M. Amjadi and M. Sitti, *ACS Nano*, 2016, **10**, 10202–10210.
147 W.-H. Chu, M. Mehregany and R. L. Mullen, *J. Micromech. Microeng.*, 1993, **3**, 4.
148 L. T. de Haan, V. Gimenez-Pinto, A. Konya, T. S. Nguyen, J. M. Verjans, C. Sánchez-Somolinos, J. V. Selinger, R. L. Selinger, D. J. Broer and A. P. Schenning, *Adv. Funct. Mater.*, 2014, **24**, 1251–1258.
149 Z. Huang, G. C.-P. Tsui, Y. Deng, C.-Y. Tang, M. Yang, M. Zhang and W.-Y. Wong, *J. Mater. Chem. C*, 2022, **10**, 12731–12740.
150 D. Jayoti, A. R. Peeketi, R. K. Annabattula and S. K. Prasad, *Soft Matter*, 2022, **18**, 3358–3368.
151 J. Wang, B. Yang, M. Yu and H. Yu, *ACS Appl. Mater. Interfaces*, 2022, **14**, 15632–15640.
152 Y. Yu, L. Li, E. Liu, X. Han, J. Wang, Y.-X. Xie and C. Lu, *Carbon*, 2022, **187**, 97–107.
153 Y. Deng, F. Zhang, M. Jiang, Y. Liu, H. Yuan and J. Leng, *ACS Appl. Mater. Interfaces*, 2022, **14**, 42568–42577.
154 Y. Li, X. Xie, Q. Zhu, S. Lu and Y. Bai, *J. Mater. Chem. A*, 2022, **10**, 22205–22213.
155 D. Okawa, S. J. Pastine, A. Zettl and J. M. Fréchet, *J. Am. Chem. Soc.*, 2009, **131**, 5396–5398.
156 C. Maggi, F. Saglimbeni, M. Dipalo, F. De Angelis and R. Di Leonardo, *Nat. Commun.*, 2015, **6**, 7855.
157 M. Liao, H. Sun, X. Tao, X. Xu, Z. Li, X. Fu, S. Xie, L. Ye, Y. Zhang and B. Wang, *ACS Appl. Mater. Interfaces*, 2018, **10**, 26765–26771.
158 D. Pan, D. Wu, P. J. Li, S. Y. Ji, X. Nie, S. Y. Fan, G. Y. Chen, C. C. Zhang, C. Xin and B. Xu, *Adv. Funct. Mater.*, 2021, **31**, 2009386.
159 Y. Zheng and C. Li, *Giant*, 2023, **16**, 100192.
160 X. Zhou, Z. Li, L. Tan, Y. Zhang and Y. Jiao, *ACS Appl. Mater. Interfaces*, 2020, **12**, 23134–23144.
161 R. Chen, H. Zhang, Y. Du, H. Ma, X. Ma, J. Ji, X. Wang and M. Xue, *Small*, 2024, 2309130.
162 Y. Wang, Y. Dong, F. Ji, J. Zhu, P. Ma, H. Su, P. Chen, X. Feng, W. Du and B.-F. Liu, *Sens. Actuators, B*, 2021, **347**, 130613.
163 Z. Zhang, F. Zhang, W. Jian, Y. Chen and X. Feng, *ACS Appl. Mater. Interfaces*, 2024, **16**, 23914–23923.
164 L. Dai, Z. Ge, N. Jiao and L. Liu, *Small*, 2019, **15**, 1902815.
165 T. Luan, F. Meng, P. Tao, W. Shang, J. Wu, C. Song and T. Deng, *Small*, 2019, **15**, 1804959.
166 S. V. Ahir and E. M. Terentjev, *Nat. Mater.*, 2005, **4**, 491–495.
167 Y. Hu, J. Liu, L. Chang, L. Yang, A. Xu, K. Qi, P. Lu, G. Wu, W. Chen and Y. Wu, *Adv. Funct. Mater.*, 2017, **27**, 1704388.
168 X. Wang, P. Xue, S. Ma, Y. Gong and X. Xu, *ACS Appl. Mater. Interfaces*, 2023, **15**, 49689–49700.
169 M. Li, F. Zhu, Y. Ge, J. Zhou, X.-M. Chen, W. Chen and N. Li, *ACS Mater. Lett.*, 2023, **5**, 1841–1850.
170 J. Li, R. Zhang, L. Mou, M. J. de Andrade, X. Hu, K. Yu, J. Sun, T. Jia, Y. Dou and H. Chen, *Adv. Funct. Mater.*, 2019, **29**, 1808995.
171 M. Gu and T. J. Echtermeyer, *Small*, 2024, 2311001.
172 L. Yang, K. Setyowati, A. Li, S. Gong and J. Chen, *Adv. Mater.*, 2008, **20**, 2271–2275.
173 X. Liu, R. Wei, P. T. Hoang, X. Wang, T. Liu and P. Keller, *Adv. Funct. Mater.*, 2015, **25**, 3022–3032.
174 Z. Li, Y. Yang, Z. Wang, X. Zhang, Q. Chen, X. Qian, N. Liu, Y. Wei and Y. Ji, *J. Mater. Chem. A*, 2017, **5**, 6740–6746.
175 H. Tian, Z. Wang, Y. Chen, J. Shao, T. Gao and S. Cai, *ACS Appl. Mater. Interfaces*, 2018, **10**, 8307–8316.
176 L. Liu, M.-H. Liu, L.-L. Deng, B.-P. Lin and H. Yang, *J. Am. Chem. Soc.*, 2017, **139**, 11333–11336.
177 M. P. Da Cunha, M. G. Debije and A. P. Schenning, *Chem. Soc. Rev.*, 2020, **49**, 6568–6578.
178 M. P. Da Cunha, E. A. van Thoor, M. G. Debije, D. J. Broer and A. P. Schenning, *J. Mater. Chem. C*, 2019, **7**, 13502–13509.
179 Z. Han, Y. Li, X. Wu and J. Zhang, *ACS Appl. Mater. Interfaces*, 2024, **16**, 14345–14356.
180 Y. Liu, H. Gu, Y. Jia, J. Liu, H. Zhang, R. Wang, B. Zhang, H. Zhang and Q. Zhang, *Chem. Eng. J.*, 2019, **356**, 318–328.
181 K. Zheng, J. Zhang, H. Dodiuk, S. Kenig, C. Barry, H. Sun and J. Mead, *ACS Appl. Polym. Mater.*, 2020, **2**, 1614–1622.
182 F. Guo, Q. Wen, Y. Peng and Z. Guo, *J. Colloid Interface Sci.*, 2017, **494**, 54–63.
183 Y. Zhong, L. Gu, S. Wang, Y. Jin and H. Xiao, *Ind. Eng. Chem. Res.*, 2019, **58**, 20323–20330.
184 B. Li, S. Xue, P. Mu and J. Li, *ACS Appl. Mater. Interfaces*, 2022, **14**, 30192–30204.
185 Y. Zhu, F. Sun, H. Qian, H. Wang, L. Mu and J. Zhu, *Chem. Eng. J.*, 2018, **338**, 670–679.
186 R. S. Sutar, X. Wu, S. S. Latthe, B. Shi, R. Xing and S. Liu, *J. Environ. Chem. Eng.*, 2023, **11**, 111299.
187 B. Chen, R. Zhang, H. Fu, J. Xu, Y. Jing, G. Xu, B. Wang and X. Hou, *Sci. Rep.*, 2022, **12**, 2187.
188 X. Dong, S. Gao, J. Huang, S. Li, T. Zhu, Y. Cheng, Y. Zhao, Z. Chen and Y. Lai, *J. Mater. Chem. A*, 2019, **7**, 2122–2128.
189 X. Liu, X. Zhang, Q. Chen, Y. Pan, C. Liu and C. Shen, *Chem. Eng. J.*, 2021, **406**, 126532.

190 X. Wang, N. Jiao, S. Tung and L. Liu, *ACS Appl. Mater. Interfaces*, 2019, **11**, 30290–30299.
191 S. P. Dalawai, M. A. S. Aly, S. S. Latthe, R. Xing, R. S. Sutar, S. Nagappan, C.-S. Ha, K. K. Sadasivuni and S. Liu, *Prog. Org. Coat.*, 2020, **138**, 105381.
192 R.-L. Yang, Y.-J. Zhu, F.-F. Chen, D.-D. Qin and Z.-C. Xiong, *ACS Sustain. Chem. Eng.*, 2019, **7**, 13226–13235.
193 H. Wu, J. Luo, X. Huang, L. Wang, Z. Guo, J. Liang, S. Zhang, H. Xue and J. Gao, *J. Colloid Interface Sci.*, 2021, **603**, 282–290.
194 J. Chen, Z. Zhu, H. Zhang and S. Fu, *Compos. Sci. Technol.*, 2022, **220**, 109278.
195 X. Song, X. Huang, J. Luo, B. Long, W. Zhang, L. Wang, J. Gao and H. Xue, *Nanoscale*, 2021, **13**, 12017–12027.
196 X. Fan, Y. Wang, Y. Xie, Z. Xiao and H. Wang, *Chem. Eng. J.*, 2024, **479**, 147614.
197 X. Song, H. Wu, Y. Zhang, G. Zhang, H. Xue and J. Gao, *Colloids Surf., A*, 2023, **673**, 131737.
198 X. Su, H. Li, X. Lai, Z. Yang, Z. Chen, W. Wu and X. Zeng, *J. Mater. Chem. A*, 2018, **6**, 16910–16919.
199 R.-L. Yang, Y.-J. Zhu, D.-D. Qin and Z.-C. Xiong, *ACS Appl. Mater. Interfaces*, 2019, **12**, 1339–1347.
200 X. Wang, L. Dai, N. Jiao, S. Tung and L. Liu, *Chem. Eng. J.*, 2021, **422**, 129394.
201 X. D. Sun, H. Yang, Y. Liang, K. Yan, L. Liu, D. Gao and J. Ma, *ACS Appl. Mater. Interfaces*, 2023, **15**, 43205–43215.
202 X. Yang, Y. Chen, X. Zhang, P. Xue, P. Lv, Y. Yang, L. Wang and W. Feng, *Nano Today*, 2022, **43**, 101419.
203 Z. Su, Y. Zhao, Y. Huang, C. Xu, X. Yang, B. Wang, B. Xu, S. Xu and G. Bai, *Nano Res.*, 2023, **16**, 1313–1319.
204 T. Li, W. Jiang, J. Han, D. Niu, H. Liu and B. Lu, *Langmuir*, 2020, **36**, 14728–14736.
205 G. Lu, G. Zhu, B. Peng, R. Zhao, F. Shi and M. Cheng, *ACS Appl. Mater. Interfaces*, 2023, **15**, 23980–23988.
206 J. F. Campbell and H. K. Kaya, *Nature*, 1999, **397**, 485–486.
207 G. Farley, M. Wise, J. Harrison, G. Sutton, C. Kuo and S. Patek, *J. Exp. Biol.*, 2019, **222**, jeb201129.
208 L. Xu, F. Xue, H. Zheng, Q. Ji, C. Qiu, Z. Chen, X. Zhao, P. Li, Y. Hu and Q. Peng, *Nano Energy*, 2022, **103**, 107848.
209 B. Lei, Z.-Y. Wen, H.-K. Wang, J. Gao and L.-J. Chen, *ACS Appl. Mater. Interfaces*, 2023, **16**, 1596–1604.
210 M. Li, X. Wang, B. Dong and M. Sitti, *Nat. Commun.*, 2020, **11**, 3988.
211 Y. Zhao, Q. Li, Z. Liu, Y. Alsaid, P. Shi, M. K. Jawed and X. He, *Sci. Robot.*, 2023, **8**, eadf4753.
212 Y. C. Cheng, H. C. Lu, X. Lee, H. Zeng and A. Priimagi, *Adv. Mater.*, 2020, **32**, 1906233.
213 D. Zhang, K. Yang, X. Liu, M. Luo, Z. Li, C. Liu, M. Li, W. Chen and X. Zhou, *Chem. Eng. J.*, 2022, **450**, 138013.
214 P. Xue, C. Valenzuela, S. Ma, X. Zhang, J. Ma, Y. Chen, X. Xu and L. Wang, *Adv. Funct. Mater.*, 2023, **33**, 2214867.
215 X. Li, Y. Du, C. Xiao, X. Ding, X. Pan, K. Zheng, X. Liu, L. Chen, Y. Gong and M. Xue, *Adv. Funct. Mater.*, 2024, **34**, 2310380.
216 W. Liu, Z. Lei, W. Xing, J. Xiong, Y. Zhang, P. Tao, W. Shang, B. Fu, C. Song and T. Deng, *ACS Nano*, 2023, **17**, 16123–16134.
217 D. Wu, X. Li, Y. Zhang, X. Cheng, Z. Long, L. Ren, X. Xia, Q. Wang, J. Li and P. Lv, *Adv. Sci.*, 2024, 2400557.
218 J. Liu, L. Xu, Q. Ji, L. Chang, Y. Hu, Q. Peng and X. He, *Adv. Funct. Mater.*, 2024, **34**, 2310955.
219 Y. Huang, C. Su, Q. Yu, J. Jiang, N. Chen and H. Shao, *J. Sci.: Adv. Mater. Devices*, 2022, **7**, 100412.
220 H. Yang, D. Wu, S. Zheng, Y. Yu, L. Ren, J. Li, H. Ke, P. Lv and Q. Wei, *ACS Appl. Mater. Interfaces*, 2024, **16**, 9313–9322.
221 J. Huang, X. Yu, L. Li, W. Wang, H. Zhang, Y. Zhang, J. Zhu and J. Ma, *ACS Nano*, 2024, **18**, 2006–2016.
222 Z. Ling, J. Chen, S. Li, H. Lu, J. Du, Z. Liu and J. Qiu, *Chem. Eng. J.*, 2024, **485**, 150094.
223 X. Li, X. Ding, Y. Du, C. Xiao, Y. Wang, K. Zheng, X. Liu, L. Chen, X. Tian and X. Zhang, *J. Mater. Chem. C*, 2022, **10**, 14255–14264.
224 G. Tian, R. Wen, J. Ma and C. Fu, *Sens. Actuators, B*, 2024, **409**, 135586.
225 D. Kim, H. Kim, E. Lee, K. S. Jin and J. Yoon, *Chem. Mater.*, 2016, **28**, 8807–8814.
226 Y. Li, Y. Liu and D. Luo, *Adv. Opt. Mater.*, 2021, **9**, 2001861.
227 J. Xu, N. Zhao, B. Qin, M. Qu, X. Wang, B. Ridi, C. Li and Y. Gao, *ACS Appl. Mater. Interfaces*, 2021, **13**, 44833–44843.
228 F. Meder, G. A. Naselli, A. Sadeghi and B. Mazzolai, *Adv. Mater.*, 2019, **31**, 1905671.
229 M. Yang, Y. Xu, X. Zhang, H. K. Bisoyi, P. Xue, Y. Yang, X. Yang, C. Valenzuela, Y. Chen and L. Wang, *Adv. Funct. Mater.*, 2022, **32**, 2201884.
230 Z. Xu, D.-W. Wei, R.-Y. Bao, Y. Wang, K. Ke, M.-B. Yang and W. Yang, *ACS Appl. Mater. Interfaces*, 2022, **14**, 22521–22530.
231 J. Zhang, S. Liu, X. Wang, X. Zhang, X. Hu, L. Zhang, Q. Sun and X. Liu, *Mater. Horiz.*, 2024, **11**, 2483–2493.